

# Ru<sup>II</sup> Multinuclear Metallosupramolecular Rack-Type Architectures of Polytopic Hydrazone-Based Ligands: Synthesis, Structural Features, Absorption Spectra, Redox Behavior, and Near-Infrared Luminescence

Adrian-Mihail Stadler,<sup>[a, b]</sup> Fausto Puntoriero,<sup>[c]</sup> Francesco Nastasi,<sup>[c]</sup> Sebastiano Campagna,<sup>\*[c]</sup> and Jean-Marie Lehn<sup>\*[a]</sup>

*This work is dedicated to Jean-Pierre Sauvage, on the occasion of his 65th birthday*

**Abstract:** A novel class of polytopic hydrazone-based ligands was synthesized. They gave heteroleptic Ru<sup>II</sup> polynuclear rack-like complexes of formula [Ru<sub>n</sub>terpy<sub>n</sub>(bridging molecular strand)]<sup>2n+</sup> (terpy = 2,2':6',2''-terpyridine). The new rack-like systems can be viewed as being made of two identical or roughly identical peripheral subunits separated by several similar metal-containing spacer subunits. The presence of pyrazine or pyrimidine units within the molecular multitopic strands introduces additional chemical diversity: whereas a pyrimidine unit leads to appended orthogonal subunits that are on the same side with regard to the main molecular strand, a pyrazine unit leads to orthogonal subunits

that lie on different sides. Mixing pyrazine and pyrimidine units within the same (bridging) molecular strand also allows peculiar and topographically controlled geometries to be obtained. Redox studies provided evidence that each species undergoes reversible redox processes at mild potentials, which can be assigned to specific subunits of the multicomponent arrays. Non-negligible electronic coupling takes place among the various subunits, and some electron delocalization ex-

tending over the overall bridging molecular strand takes place. In particular, oxidation data suggest that the systems can behave as p-type “molecular wires” and reduction data indicate that n-type electron conduction can occur within the multimetallic framework. All the multinuclear racks exhibit <sup>3</sup>MLCT emission, both at 77 K in rigid matrix and at 298 K in fluid solution, which takes place in the near-infrared region (emission maxima in the 1000–1100 nm region), and is quite structured. Rigidity of the molecular structures and delocalization within the large bridging ligands are proposed to contribute to the occurrence of the rather uncommon MLCT infrared emission, which is potentially interesting for optical communication devices.

**Keywords:** luminescence • molecular racks • molecular wires • N ligands • polynuclear complexes • ruthenium • supramolecular chemistry

[a] Dr. A.-M. Stadler, Prof. J.-M. Lehn  
ISIS-Université de Strasbourg, 8 Allée Gaspard Monge, BP 70028  
67083 Strasbourg cedex (France)  
Fax: (+33) 390-245-140  
E-mail: lehn@isis.u-strasbg.fr

[b] Dr. A.-M. Stadler  
Karlsruhe Institute of Technology (KIT)  
Forschungszentrum Karlsruhe (FZK)  
Institute for Nanotechnology (INT)  
Postfach 3640, 76021 Karlsruhe (Germany)

[c] Dr. F. Puntoriero, F. Nastasi, Prof. S. Campagna  
Dipartimento di Chimica Inorganica  
Chimica Analitica e Chimica Fisica  
Università di Messina, Via Sperone 31, 98166 Messina (Italy)  
Fax: (+39) 090-393-756  
E-mail: campagna@unime.it

Supporting information for this article is available on the WWW under <http://dx.doi.org/10.1002/chem.200900632>.

## Introduction

Molecular racks are structurally rigid and roughly linear multicomponent species; they are made of multitopic, “programmed” molecular strands to which several suitable molecular subunits, capable to read out the coordination information encoded in the strands, are appended/complexed. The appended molecular subunits usually assume orthogonal arrangements with respect to the main molecular strand dimension.<sup>[1]</sup>

Architectures of this kind, which bring together a more or less linear sequence of metal ions, are interesting for their physical properties.<sup>[2–4]</sup> Some of them may also be used as synthetic precursors for larger architectures.<sup>[5a,b]</sup> Various metals are used in the works reported in the literature:

$\text{Ru}^{\text{II}}$ ,<sup>[2,3]</sup>  $\text{Cu}^{\text{I}}$ ,<sup>[5a,b]</sup>  $\text{Zn}^{\text{II}}$ ,<sup>[5c]</sup>  $\text{Cu}^{\text{II}}$ ,<sup>[5d]</sup>  $\text{Eu}^{\text{III}}$ ,  $\text{La}^{\text{III}}$ , or  $\text{Y}^{\text{III}}$ .<sup>[4]</sup> The rigid structure of the molecular racks is not a necessary prerequisite of the molecular strand (which plays the role of a multi-topic bridging ligand), but it can emerge upon racks formation following the coordination of the appended subunits. This is the case of molecular racks made of hydrazone-based molecular strands,<sup>[6]</sup> such as the species studied here.

Hydrazone-based molecular racks have several unusual properties compared to the formerly investigated molecular racks based on ligand strands containing exclusively terpyridine-like coordination sites.<sup>[3]</sup> 1) The synthetic routes are

easier and milder and 2) superior chemical diversity can be synthetically introduced, as various isomeric possibilities involving the position of the hydrazoneic C=N bond within the molecular strands are possible. Recently we reported the synthesis, characterization, as well as the study of the absorption spectra, luminescence properties, and redox behavior of some dinuclear  $\text{Ru}^{\text{II}}$  molecular racks based on hydrazone-based strands.<sup>[2a]</sup> Here we extend this study to larger molecular racks, spanning nuclearities from two to six (complexes **1–4,6**; Figure 1).

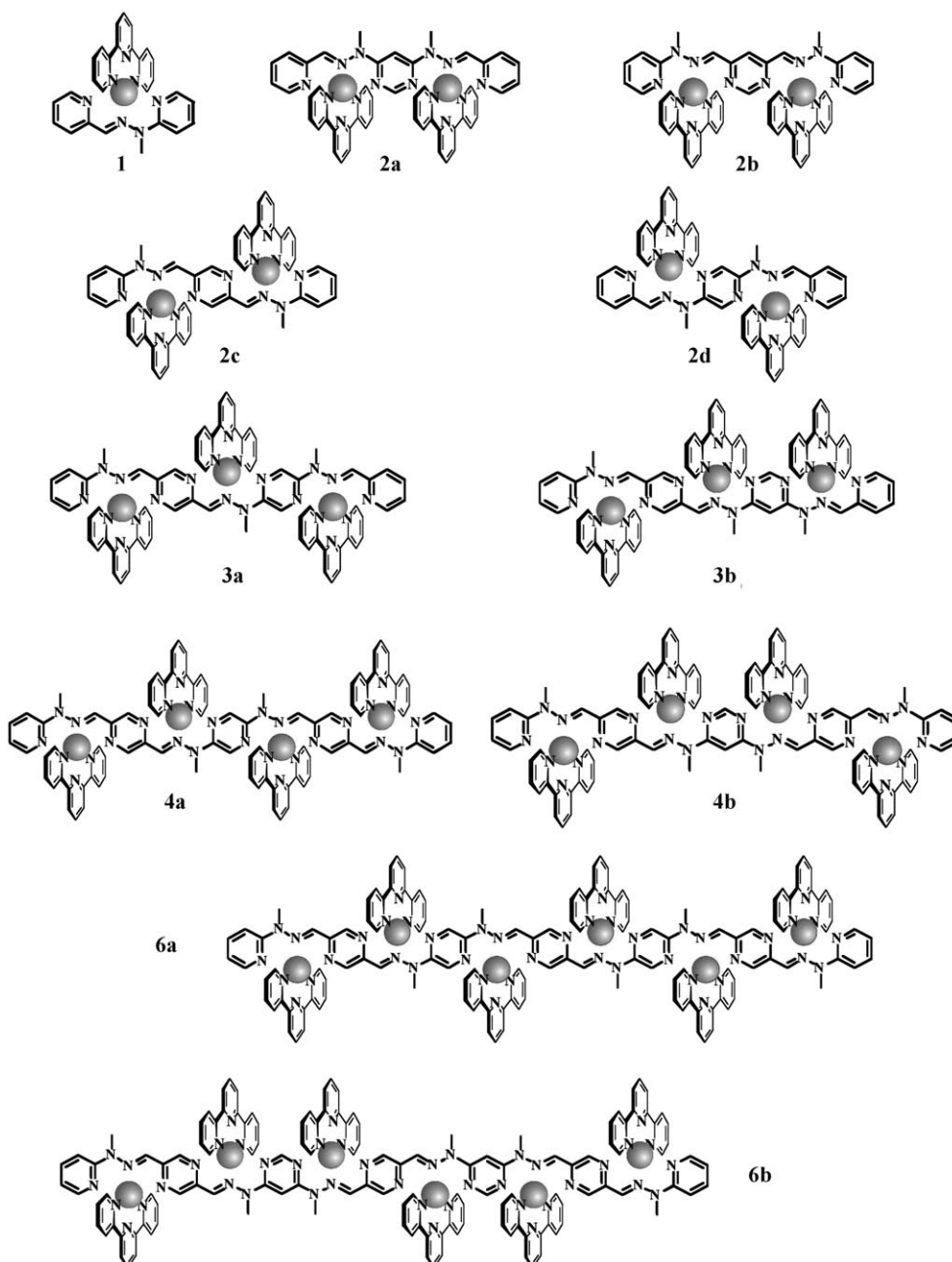


Figure 1. Structural formulae of the metal complexes (charges omitted). Complexes **2a–c** were studied previously<sup>[2a]</sup> and are reported for comparison. Synthesis and characterization of **1** and **4b** are reported, but the absorption, luminescence, and redox properties of these species were not studied for technical reasons.

The new species are based on photo- and redox-active Ru(terpy)<sup>2+</sup> subunits (terpy = 2,2':6',2''-terpyridine) appended to polytopic, molecular strands of increasing size, containing hydrazone-based terpy-type coordination centers. They can be viewed as being made of two identical (or quasi-identical, in the case of **3a** and **3b**), peripheral subunits separated by zero (the dinuclear species, **2d**), one (the trinuclear species, **3a** and **3b**), two (the tetranuclear species, **4a** and **4b**), and four (the hexanuclear compounds, **6a** and **6b**) similar metal-containing spacer subunits. The presence of pyrazine or pyrimidine units within the molecular strands also introduces a source of additional chemical diversity: actually, whereas a pyrimidine unit leads to orthogonal subunits which are on the same side with regard to the main molecular strand, a pyrazine unit leads to orthogonal subunits that lie on different sides ("alternate" racks). Mixing pyrazine and pyrimidine units within the same (bridging ligand) molecular strand leads to quite unusual and topographically controlled geometries. An example is the comparison of the structures of the hexanuclear **6a** and **6b** molecular racks.

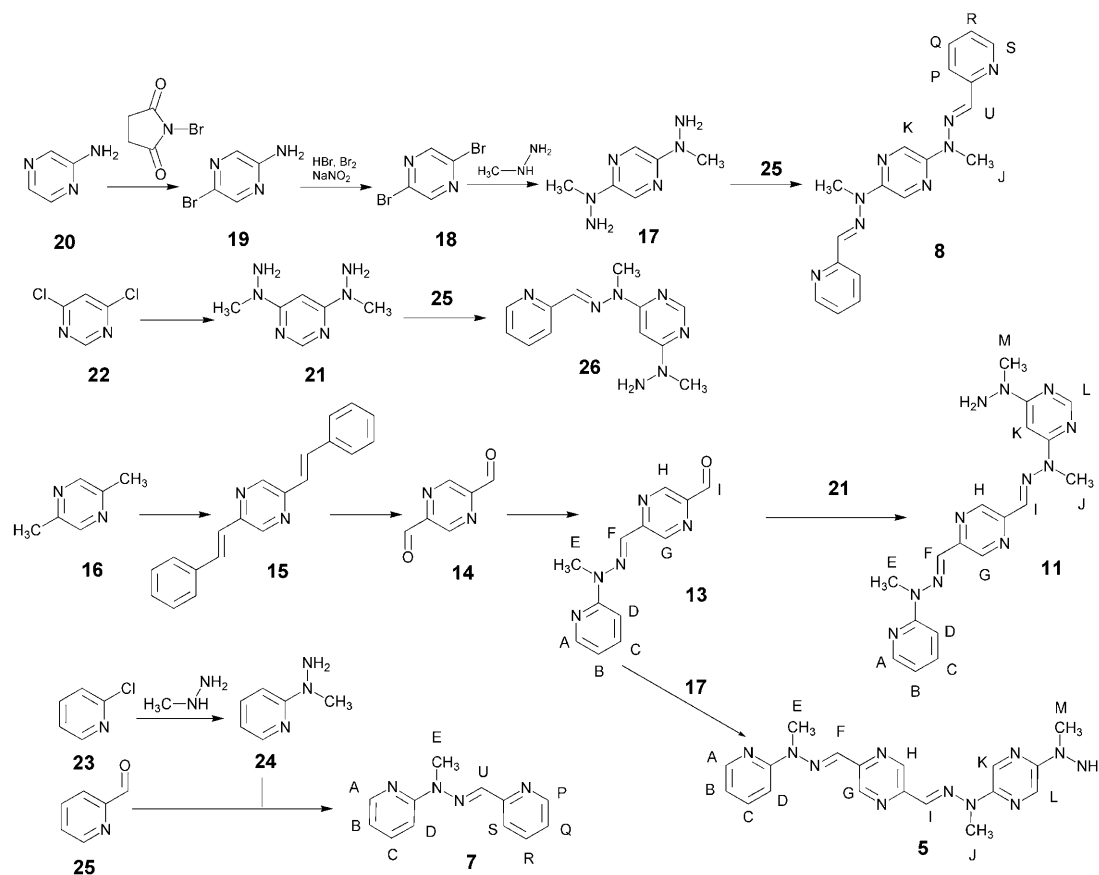
## Results and Discussion

### Synthetic approach and characterization

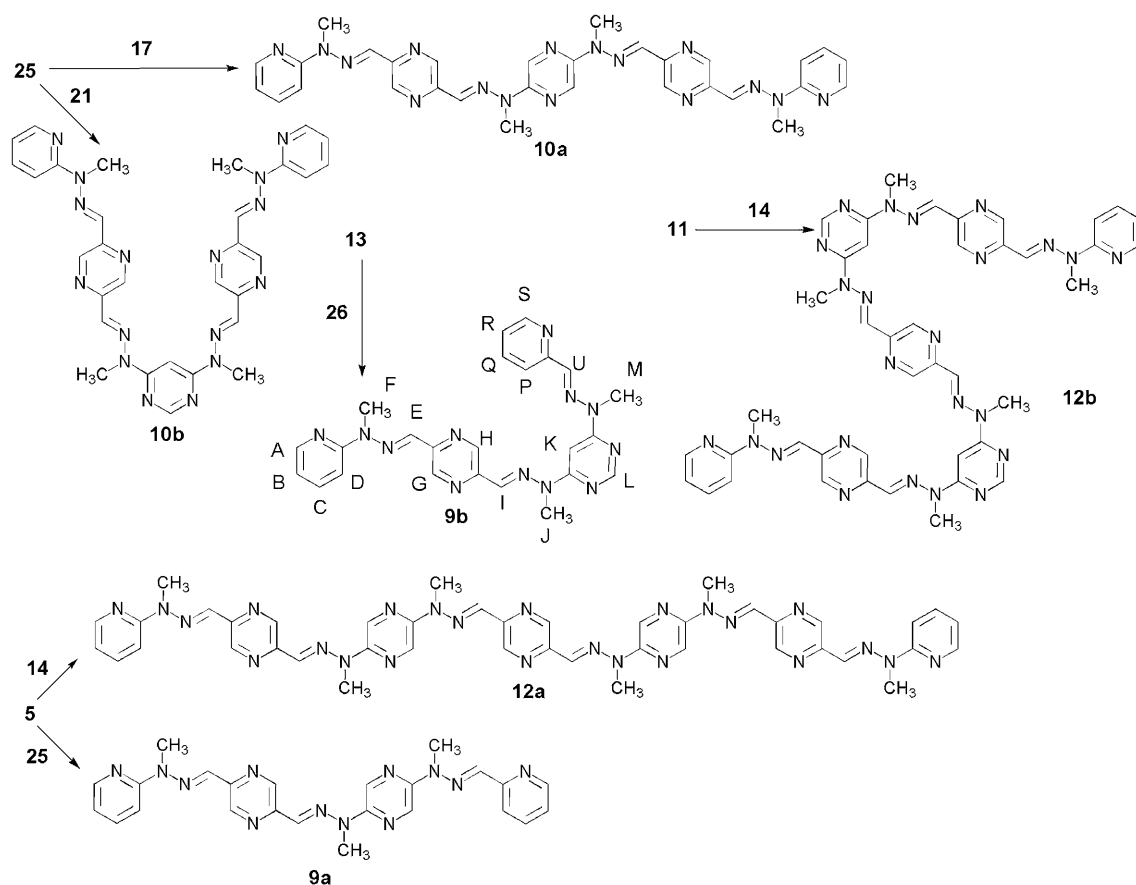
*Synthesis of ligands:* Ligand **7** was synthesized (Scheme 1) as previously described,<sup>[7]</sup> by condensation of 2-pyridinecarboxaldehyde (**25**) with 2-(1-methylhydrazino)pyridine (**24**), obtained from 2-chloropyridine (**23**) and methylhydrazine.<sup>[8]</sup>

Reaction of aminopyrazine **20** with *N*-bromosuccinimide led to 2-amino-5-bromo-pyrazine<sup>[9]</sup> (**19**), which, on treatment with Br<sub>2</sub>, HBr, and NaNO<sub>2</sub>, yielded 2,5-dibromopyrazine<sup>[10]</sup> (**18**), the reaction of which with methylhydrazine led to 2,5-bis(1-methylhydrazino)pyrazine (**17**). Reaction of **17** with two equivalents of 2-pyridinecarboxaldehyde (**25**) led to ligand **8** (Scheme 1).

The reaction of 2,5-dimethylpyrazine (**16**) with benzaldehyde, in the presence of benzoic anhydride, gave 2,5-distyrylpyrazine<sup>[11]</sup> (**15**), the ozonolysis (O<sub>3</sub>, MeOH, -78 °C) of which followed by reduction with an aqueous solution of sodium metabisulfite (Na<sub>2</sub>S<sub>2</sub>O<sub>5</sub>) produced 2,5-pyrazinedicarboxaldehyde<sup>[12]</sup> (**14**). Condensation of an excess of dialdehyde **14** with one equivalent of 2-(1-methylhydrazino)pyridine (**24**) in EtOH, at room temperature, gave the monoaldehyde **13**. Precursor **13** reacted with an excess of bishydrazine **17** or **21** to give precursors **5** or **11**, respectively (Scheme 1).



Scheme 1. Synthesis of the heterocyclic building blocks **14**, **15**, **17–19**, **21**, and **24**, of the precursors **5**, **11**, **13**, and **26** and of the ligands **7** and **8**.



Scheme 2. Synthesis of the ligands **9a,b** and **12a,b**.

Ligands **10a** and **10b** (Scheme 2) were synthesized by a double chain-extension method<sup>[13]</sup> consisting of the condensation of one equivalent of 2,5-bis(1-methylhydrazino)pyrazine (**17**) or 4,6-bis(1-methylhydrazino)pyrimidine (**21**) with two equivalents of precursor **13**. Strand **10a** has an inversion center, whereas **10b** has a  $C_2$  axis as symmetry element. Ligands **10a,b** are insoluble in organic solvents, but their  $Ru^{II}$  rack-like complexes are soluble in acetonitrile.

A double chain-extension reaction of two equivalents of **5** and **11** with 2,5-pyrazinedicarboxaldehyde (**14**) yielded ligand strands **12a** and **12b** (Scheme 2). 2-Pyridinecarboxaldehyde (**25**) reacted with one equivalent of precursor **5** and yielded the ligand strand **9a**. Reaction of precursor **13** with precursor **26**<sup>[6]</sup> [obtained from 2-pyridinecarboxaldehyde (**25**) and an excess of 4,6-bis(1-methylhydrazino)pyrimidine (**21**), see Scheme 1] gave ligand **9b**.

In these ligands, the hydrazone group is the isomorphous equivalent<sup>[14]</sup> of a 2,6-disubstituted pyridine ring.

**Synthesis of complexes:**  $Ru^{II}$  rack-type complexes may be formed by octahedral coordination of  $Ru^{II}$  with three nitrogen atoms of a terpy ligand and three of a hydrazone site (py/pz/pym-hyz-pym/pz), so that, for example, a dihydrazone ligand could generate a dinuclear complex.

The complexes were prepared following a previously described pathway for the synthesis of  $Ru^{II}$  racks.<sup>[3a-d]</sup>  $[Ru(terpy)Cl_3]^{[15]}$  was reacted with ligands **7**, **8**, **9a,b**, **10a,b**, and **12a,b** in molar ratios described in the Experimental Section, at reflux temperature, in mixtures of water and ethanol that have reducing properties (donor of electrons for the process  $Ru^{III} + e^- \rightarrow Ru^{II}$ ). The reactants were heated at reflux for 18–21 h. The results showed that the hydrazone bonds were stable under these conditions.

The complexes thus obtained had chlorides as counterions and were water soluble. They were precipitated from water by the addition of aqueous solutions of ammonium hexafluorophosphate ( $NH_4PF_6$ ). Further purification was performed by reprecipitation from  $CH_3CN$  with  $Et_2O$  or chloroform.

The complexes are colored solid materials (**1** and **2d** are brown, the others are deep green), soluble in acetonitrile or acetone, but insoluble in toluene, diethyl ether, diisopropyl ether, benzene, or chloroform, properties that were used in crystallization experiments to obtain single crystals.

**Crystallographic studies:** Single crystals suitable for X-ray diffraction were obtained by slow diffusion of  $Et_2O$  into a solution of complex **1** or **2d** in  $CH_3CN$ . Both crystals are monoclinic. The expected structures (Figure 2) were con-



tons E) display similar  $^1\text{H}$  NMR resonances. Racks contain a determined number of types of terpy: one type (**1**, **2d**), two types (**4a**, **4b**), or three types (**3a**, **3b**, **6a**, **6b**). This is confirmed by  $^1\text{H}$  NMR data and also by  $^{13}\text{C}$  NMR data, as shown in Figure 6, in the case of carbon C5 of the terminal pyridines of the terpy units.

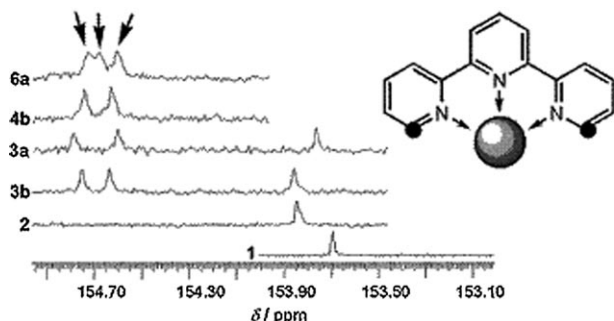


Figure 6.  $^{13}\text{C}$  NMR spectra of the region containing the peaks of C5 (●) of the monosubstituted pyridines in complexes **2d**, **3b**, **3a**, **4b**, and **6a** (75 MHz,  $\text{CD}_3\text{CN}$ ).

The coordination induces conformational changes. For example, it causes  $\text{C4pym-Nsp}^3$ ,  $\text{C6pym-Nsp}^3$ ,  $\text{C2pz-Nsp}^3$ ,  $\text{C5pz-Nsp}^3$ , and  $\text{C2py-Nsp}^3$  bonds to turn on their axes, and the place of the  $\text{Nsp}^3\text{-Nsp}^2$  bond is taken by the  $\text{Nsp}^3\text{-CH}_3$  bond. It also causes the  $\text{C2pz-Csp}_{\text{hyz}}^2$ ,  $\text{C5pz-Csp}_{\text{hyz}}^2$ , and  $\text{C2py-Csp}_{\text{hyz}}^2$  bonds to turn, and the place of the  $\text{Csp}_{\text{hyz}}^2=\text{Nsp}^2$  bond is taken by the  $\text{Csp}_{\text{hyz}}^2\text{-H}$  bond.

The shapes of the coordinated strands as represented in the structural formulae are confirmed by 2D NMR spectroscopy, essentially by correlations due to the existence of NOEs between several key protons closely involved in the conformational change of the ligand before and after binding of the metal ion. The coordination induces the transformation of the *all-transoid* conformation into an *all-cisoid* one. In the case of terpy, it produces the  $(\text{T}_4, \text{T}_5)$  NOE observed for all complexes. The shape of the coordinated ligand is established by NOEs, which do not exist in the free ligand, but appear after coordination, such as the following: (D,E), (F,G), (H,I), (J,K), ( $\text{K}_{\text{pym}}, \text{M}$ ), (J,K), ( $\text{L}_{\text{pz}}, \text{M}$ ), (P,U). Thus, the following NOEs were observed for **4a**: (D,E), (F,G), (H,I), (J,K) (Figure 7).

The DOSY spectrum (Figure 8) of an equimolar mixture of complexes **1**, **2d**, **3b**, **4b**, and **6b** resulted in the determination of five diffusion coefficients with the following values: 967, 686, 579, 503, 440  $\mu\text{m}^2\text{s}^{-1}$ . The diffusion coefficient exponentially decreases with increasing nuclearity. A similar evolution was observed in the case of a series of  $[\text{Ru}^{\text{II}}_{n-1}\{\text{methylphenylenebis(terpyridine)}\}_n]$  ( $n=2-6$ ) oligomers formed in a single-pot reaction,<sup>[16a]</sup> as well as a series of helicates of increasing nuclearity.<sup>[16b]</sup>

### Redox behavior

**Oxidation:** Recently, we partly reported the oxidation properties of **2c**, **3a**, **4a**, and **6a**, and the results obtained allowed

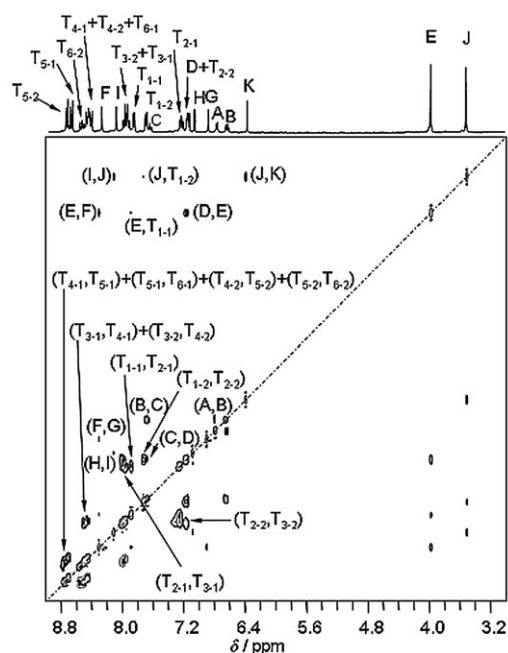


Figure 7.  $^1\text{H}$ - $^1\text{H}$  NOESY spectrum of complex **4a** (300 MHz,  $\text{CD}_3\text{CN}$ ).

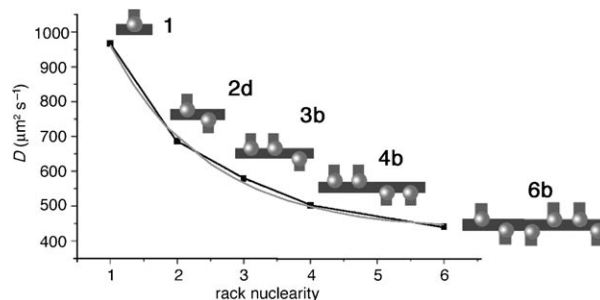


Figure 8. Dependence of the diffusion coefficients obtained by DOSY on the nuclearity of the complexes.

us to calculate an electronic coupling attenuation parameter (usually called  $\beta$ ) for the inner metal-based modules.<sup>[2b]</sup> The relatively low  $\beta$  parameter obtained (0.23  $\text{\AA}^{-1}$ ) indicates that these molecular racks exhibit p-type “molecular wire” properties of potential interest for implementation in supramolecular electronic devices.<sup>[2b,17]</sup> Here we describe the complete oxidation behavior of all the rack species studied.

The oxidation patterns of the  $\text{Ru}^{\text{II}}$  rack complexes show several processes (Table 2, Figure 9), most of them reversible, that can be classified as metal-centered, on the basis of literature data.<sup>[18]</sup> The dinuclear species **2d** shows two metal-centered oxidation processes, separated by 250 mV. This potential splitting is connected to the electronic coupling between the two metal-based orbitals, mediated by superexchange through the  $\text{-N-pyrazine-N-}$  bridging-moiety orbitals, by taking advantage of both HOMO and LUMO orbitals of the bridge.<sup>[2a]</sup> Electrostatic terms can also contribute to the interaction. The potential splitting in **2d** is in line with that found for the already investigated **2a-c** racks, the redox properties of which are also shown in Table 2 for

Table 2. Spectroscopic and redox data.

	Absorption <sup>[a]</sup>		Luminescence		Redox data <sup>[a,c]</sup>	
	298 K	77 K <sup>[b]</sup>	298 K <sup>[a]</sup>	77 K <sup>[b]</sup>	$E_{1/2}$ ox	$E_{1/2}$ red
	$\lambda_{\max}$ [nm]	$\lambda_{\max}$ [nm]	$\lambda_{\max}$ [nm]	$\lambda_{\max}$ [nm]	[V vs. SCE]	[V vs. SCE]
	( $\epsilon$ [ $M^{-1} \text{cm}^{-1}$ ])	( $\tau$ [ns])	( $\tau$ [ns])	( $\tau$ [ns])		
<b>2a</b> <sup>[d]</sup>	308 (70300)	758 (30)	741 (335)		+1.28 (65)	-0.98 (62)
	330 (60300)				+1.53 (70)	-1.22 (65)
	434 (22400)				+1.78 (80)	-1.35 (70)
	470 (20700)					-1.43 (80)
<b>2b</b> <sup>[d]</sup>	330 (42500)				+1.36 (68)	-0.45 (60)
	430 (45700)				+1.66 (75)	-1.05 (65)
	506 (12600)					-1.46 (75)
	630 (27000)					-1.65 (82)
<b>2c</b> <sup>[d]</sup>	272 (56700)				+1.27 (65)	-0.50 (65)
	440 (47400)				+1.50 (70)	-1.05 (65)
	614 (40600)					-1.49 (75)
	772 (2700)					-1.57 (82)
<b>2d</b>	273 (46000)	765 (60)	750 (400)		+1.27 (72)	-0.88 (72)
	310 (65000)				+1.52 (78)	-1.42 (75)
	406 (51000)					-1.59 (80)
	437 (44000)					
<b>3a</b>	308 (79000)	1040	1038		+1.30 (90) <sup>[e]</sup>	-0.41 (65)
	447 (72000)				+1.43 (92) <sup>[e]</sup>	-0.86 (75)
	630 (47500)					-1.24 (78)
<b>3b</b>	308 (80000)	1022	1004		+1.34 (70)	-0.38 (62)
	430 (53000)				+1.45 (72)	-0.85 (70)
	631 (38000)					-1.09 (75)
<b>4a</b>	304 (118000)	1052	1048		+1.32 (65)	-0.37 (65)
	460 (86000)				+1.37 (68)	-0.47 (68)
	650 (104000)				+1.61 (75)	-0.86 (75)
	823 (11800)					-1.10 (75)
<b>6a</b>	305 (149000)	1078	1044		+1.34 (58)	-0.30 (57)
	458 (132000)				+1.43 (62)	-0.39 (62)
	664 (152000)				+1.64 (78)	
	845 (21500)					
<b>6b</b>	305 (155000)	1032	1018		+1.40 (72) <sup>[f]</sup>	-0.41 (65)
	440 (125000)				+1.54 (82)	-0.56 (72)
	659 (139000)					

[a] In argon-purged acetonitrile. [b] In MeOH/EtOH (4:1, v/v) matrix at 77 K. [c] In parentheses, the peak-to-peak separations for the redox couples are given, in mV. [d] From reference [2a]. [e] Quasi-reversible process. [f] Bi-electronic process.

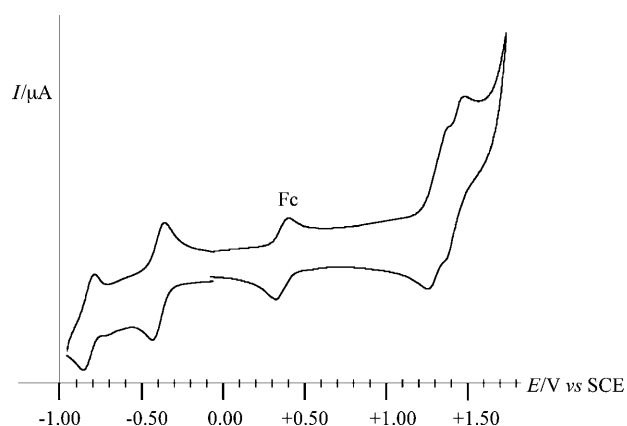


Figure 9. Cyclic voltammogram of **3b** in acetonitrile solution. The wave at about 0.4 V is ferrocene (Fc), used as an internal standard.

comparison purposes, and this suggests that the metal–metal interaction is roughly similar within the series of dinuclear species.<sup>[2a,19–22]</sup>

The oxidation pattern of the trinuclear systems **3a** and **3b** shows two mono-electronic processes. Whereas in the dinuclear systems the two metal centers were identical, in this case the three metal centers of each species are all different from one another, because they have different bridging ligand moieties. The clear difference is that two metal centers are peripheral, and are therefore linked to a single bridging moiety, and one is central, so linked to two bridging residues. Because the backbonding ability of a peripheral  $-\text{N}=\text{C}$ -pyridine residue is worse than that of a bridging moiety,<sup>[2a]</sup> the peripheral metal centers should have a larger electron density than the central metal center, and they would be oxidized at milder potentials. The peripheral metal centers are also different from one another. For example, in **3a** one metal is linked to an  $-\text{N}=\text{C}$ -pyrazine- $\text{C}=\text{N}-$  group, and the other to an  $-\text{N}$ -pyrazine- $\text{N}-$  bridging group (the other ligand moieties, identical for both metals, such as the terpyridine ligands, are not considered). As models for the oxidation potential of the two metal centers, we can consider the first oxidation of **2c** and **2d**, anticipating that both of them are slightly displaced to more positive potentials in the trinuclear species because of the presence of the central unit. In fact, the first oxidation process of **3a** (+1.30 V) is slightly more positive than those of **2c** and **2d**; however, one cannot decide which peripheral metal center is involved in the first oxidation process, because the oxidation potential of the models are too close (+1.28 and +1.27 V, see Table 2). The second oxidation involves the not yet oxidized peripheral metal center, and the potential splitting (130 mV) is evidently reduced compared to that occurring in the dinuclear species, because of increased separation between the redox-active centers. The identical arguments can be employed to discuss the oxidation behavior of the trinuclear species **3b**, with peripheral unit models **2a** and **2c**.

In the tetranuclear species **4a**, symmetry is restored: the two peripheral metal centers are identical, and so are the inner metal centers. The first two oxidation processes involve successive one-electron oxidation of the peripheral metal centers. The potential splitting, 50 mV, is in line with the increased distance between the redox-active sites involved, when compared to the lower nuclearity compounds. A third, irreversible process, takes place at +1.61 V, and is assigned to the oxidation of one of the two inner metal centers. Interestingly, the difference between second and third oxidation potentials, 240 mV, related to the coupling between the peripheral and inner units, is almost identical to the difference between two oxidation processes of **2c**, which contains the identical bridging moiety between the pertinent metal center units (that is, the  $-\text{N}=\text{C}$ -pyrazine- $\text{C}=\text{N}-$  unit).

The hexanuclear species **6a** and **6b** exhibit symmetric structures with respect to the central pyrazine ring. So, three types of metal centers are present in both compounds. On the basis of the discussion made for the trinuclear species, the metal centers that are expected to be oxidized at milder potentials are the two peripheral centers. Indeed, the first oxidation process of both the hexanuclear species is bi-electronic, and is assigned to the simultaneous one-electron oxi-

dation of the weakly interacting peripheral metal centers. The absence of splitting of the peripheral oxidation in the hexanuclear racks is not surprisingly: on considering the distance between the sites and the value of  $0.23 \text{ \AA}^{-1}$  calculated for the  $\beta$  parameter in the **2c**, **3a**, **4a** series, a splitting of 10 mV is estimated for **6a**,<sup>[2b]</sup> and this value is beyond detection by our differential pulse voltammetry apparatus. A further, irreversible oxidation process is present in the oxidation pattern of both **6b** and **6a**. Such a process is assigned to an inner metal center, most likely one of the two metal centers not directly linked to the already oxidized peripheral centers: the difference in potentials between the bi-electronic process and the successive, mono-electronic process (110 mV in **6a** and 140 mV in **6b**) is indeed of the same order of the difference between the two oxidation potentials in the trinuclear species (130 and 110 mV in **3a** and **3b**, respectively), supporting the assignment (in all cases, the difference in potential would be related to processes involving metal centers separated by another interposed and not yet oxidized metal center).

**Reduction:** To discuss the reduction behavior of the rack complexes, it is useful to identify the various redox-active subunits and, on the basis of the results reported for the formerly investigated dinuclear species of the same family,<sup>[2a]</sup> to make hypotheses on the probable potential range where the reduction processes of such redox-active subunits can be expected.

On reduction, we can identify the following types of subunits, going from the subunits which are expected to be reduced at milder potentials to the ones which are expected to be reduced at more negative potentials:

- 1) The  $-\text{N}=\text{C}-\text{pyrazine}-\text{C}=\text{N}-$  units, that is, the bis-chelating bridging units containing a LUMO which extends over a central pyrazine and two conjugate  $\text{C}=\text{N}$  bonds, (see genetic diagrams in Figure 10). From the information gained by the redox properties of dinuclear species,<sup>[2a]</sup> a subunit such as this should be mono-reduced at about  $-0.40 \text{ V}$  versus SCE and can be doubly reduced in the range  $-0.90$  to  $-1.25 \text{ V}$ . Note that in the tetranuclear species **4a** two identical  $-\text{N}=\text{C}-\text{pyrazine}-\text{C}=\text{N}-$  bridging units are present, each one connecting a peripheral Ru center with an inner one, and in the larger hexanuclear species two types of such units are present: two such units are located at the periphery of the supramolecular structure, connecting a terminal Ru unit with an inner Ru center, whereas one such unit connects two inner Ru centers. It is hard to predict a priori which can be the difference in redox potentials between these two types of redox-active units.
- 2) The  $-\text{N}-\text{pyrazine}-\text{N}-$  or  $-\text{N}-\text{pyrimidine}-\text{N}-$  bis-chelating units, in which the LUMO is essentially centered on the pyrazine or pyrimidine ring (see Figure 10). This type of subunit is reduced in the range  $-0.80$  to  $-0.95 \text{ V}$ .<sup>[2a]</sup>
- 3) The terpy ligands, which are mono-reduced at potentials more negative than  $-1.30 \text{ V}$ .<sup>[18]</sup> Even in this case, termi-

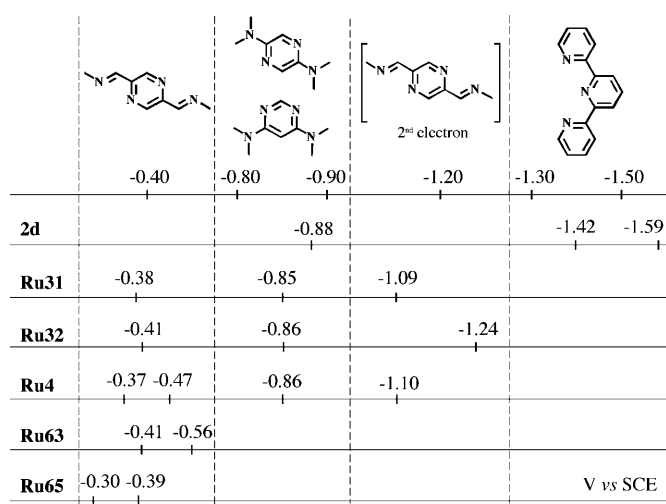


Figure 10. Schematic representation of the reduction potentials of the reported complexes. In the first row, the various redox-active subunits expected to be reduced in a potential range (vertical borders) are shown.

nal and inner locations for the various terpy ligands can be identified, and such different locations are expected to have a consequence on the electron density on the terpy (terpy ligands linked to a terminal, electronically richer Ru center should be more difficult to reduce, that is, they should be reduced at more negative potentials than terpy ligands linked to an inner, electronically poorer Ru center). Second-order differences could also be present as a consequence of the overall chemical environment of the metal center to which the various terpy ligands are linked (compare for example the two terminal terpy ligands of the trinuclear species: one is linked to a  $\text{Ru}^{\text{II}}$  center connected to a bridging delocalized  $-\text{N}=\text{C}-\text{pyrazine}-\text{C}=\text{N}-$  unit, whereas the other is linked to a  $\text{Ru}^{\text{II}}$  center which is coordinated by a bridging pyrazine/pyrimidine ring). However, also in this case it is hard to predict a priori the electronic differences among the various terpy units.

In the light of the general guidelines derived from the above-mentioned considerations, the reduction behavior of the new complexes will be discussed (Table 2; the redox properties of the dinuclear species **2a–c** are also reported for comparison). However, the analysis of the reduction behavior is complicated by the lack of reversibility of several processes. For this reason, in many cases the assignment of the reduction processes should be considered only as tentative.

The reduction pattern of **2d**, which completes the dinuclear series, corresponds to those of the formerly studied **2a–c** species: the three mono-electronic reduction processes of **2d** are straightforwardly assigned to reduction of the bridging pyrazine subunit and to reduction of the two terpy ligands. The two terpy-based reductions are split by 170 mV, indicating a significant electronic interaction between the (identical) terpy subunits.

For the trinuclear species **3a** and **3b**, the first reduction process is assigned to the  $-\text{N}=\text{C}$ -pyrazine- $\text{C}=\text{N}-$  bridging subunit and the second reduction process is assigned to the second bridging  $-\text{N}$ -pyrazine- $\text{N}-$  (in **3a**) or to the  $-\text{N}$ -pyrimidine- $\text{N}-$  (in **3b**) unit (for the sake of simplicity, from herein these subunits will be named pyrazine-based and pyrimidine-based units, respectively). The practically coincident potential of the second reduction potentials of the trinuclear species (involving a pyrimidine/pyrazine-based unit) with those occurring for the reduction of the equivalent bridging units in the corresponding dinuclear species **2c** and **2d** is most likely due to two contrasting effects. In fact, in the trinuclear species, the LUMO centered in the bridging pyrazine/pyrimidine unit should be stabilized in comparison to the dinuclear species (the inner Ru center of the trinuclear compounds should backbond mainly towards the other bridging ligand) and therefore its reduction potential should move to less negative potentials; however, first reduction on the other bridging  $-\text{N}=\text{C}$ -pyrazine- $\text{C}=\text{N}-$  unit would balance this effect. The third reduction process occurs at potentials similar to those of second reduction of the  $-\text{N}=\text{C}$ -pyrazine- $\text{C}=\text{N}-$  unit in the corresponding dinuclear species **2a** and **2b**, and therefore it is assigned to second reduction of this latter site also in the trinuclear species. At more negative potentials, terpy-based reductions take place. However, the behavior of such successive reduction processes is irregular, making it impossible to discuss them in detail.

For the tetranuclear species **4a**, the first two mono-electronic reductions are assigned to the two  $-\text{N}=\text{C}$ -pyrazine- $\text{C}=\text{N}-$  bridging units that are present. Their potential splitting (100 mV) is related to their electronic interaction through the molecular strand. The third (irreversible) process, occurring at about  $-0.86$  V versus SCE, is tentatively assigned to reduction of the inner bridging pyrazine-based unit.

The reduction pattern of the hexanuclear species shows two quasi-reversible processes, peaking, in the differential pulse voltammetry experiments, at  $-0.30$  and  $-0.39$  V for **6a** and at  $-0.43$  and  $-0.57$  V for **6b**. Successive ill-behaved and irreversible processes take place at potentials more negative than  $-0.90$  V. The irreversible nature of the reduction processes makes it impossible to carefully determine the number of electrons involved in each process. Tentatively, because the hexanuclear species contain two different types of bridging  $-\text{N}=\text{C}$ -pyrazine- $\text{C}=\text{N}-$  units, in a 1:2 ratio, and assuming that the inner bridging  $-\text{N}=\text{C}$ -pyrazine- $\text{C}=\text{N}-$  unit is easier to reduce than the peripheral  $-\text{N}=\text{C}$ -pyrazine- $\text{C}=\text{N}-$  units, at a first sight it is reasonable to assign the first process to reduction of the inner bridge and the second reduction process to simultaneous one-electron reduction of the two peripheral bridges. Alternative assignments are nonetheless possible, as will be discussed later in this section.

Independent of the detailed assignments of the two reduction processes, the LUMOs of **6a** are significantly stabilized compared to the LUMOs of **6b** (compare the first reduction potentials of the two complexes, Table 2). The difference

has to be due to the nature of the aromatic rings of the strands separating the  $-\text{N}=\text{C}$ -pyrazine- $\text{C}=\text{N}-$  units: in **6a**, it is a pyrazine-based component, and in **6b**, a pyrimidine-based component. On comparing the first reduction potential of the homologue species **2d** (reduction localized on pyrazine-based unit, occurring at  $-0.88$  V) and **2a** (reduction involving a pyrimidine-based unit, occurring at  $-0.98$  V<sup>[2a]</sup>), it appears that pyrazine-based subunits of the strands have lower-lying orbitals than pyrimidine-based subunits; this could contribute to stabilize the LUMOs involving  $-\text{N}=\text{C}$ -pyrazine- $\text{C}=\text{N}-$  units in **6a** compared to **6b**. However, it is not the mere presence of the pyrazine- versus pyrimidine-based separating unit that makes the difference, because this is not reflected by the redox properties of **3a** and **3b**.<sup>[23]</sup> Most likely, it is the electronic coupling among the three low-lying and redox-active  $-\text{N}=\text{C}$ -pyrazine- $\text{C}=\text{N}-$  units that benefits from the presence of the *para*-disubstituted pyrazine-based bridging moiety. This increased coupling leads to stabilization of all the  $-\text{N}=\text{C}$ -pyrazine- $\text{C}=\text{N}-$  units of **6a**, the LUMO of which, although mostly involving the central subunit, also receives significant contributions from both the two peripheral  $-\text{N}=\text{C}$ -pyrazine- $\text{C}=\text{N}-$  units, as a consequence of this inter-unit coupling. In other words, the LUMO of **6a** is partly delocalized over the entire molecular strand, whereas this delocalization is much lower for the LUMO of **6b**, largely localized on the central  $-\text{N}=\text{C}$ -pyrazine- $\text{C}=\text{N}-$  unit, because the *meta*-disubstituted pyrimidine-based bridging units allow only reduced coupling between the  $-\text{N}=\text{C}$ -pyrazine- $\text{C}=\text{N}-$  units they connect.

In the limiting case of complete delocalization of the LUMO within the molecular frame of **6a**, an alternative assignment of the first two reduction processes of this compound could be proposed. In this limiting case, the two processes could be both mono-electronic and ultimately lead to partial localization of the added electrons on the two peripheral  $-\text{N}=\text{C}$ -pyrazine- $\text{C}=\text{N}-$  units, so minimizing repulsion. A third electron could not be added in this case at mild potentials, because the energy of the LUMO would increase. With the data in our hands, we cannot verify the extent of LUMO delocalization within the molecular frame, so the hypothesis should be taken with care.

The case of complete delocalization, which can be valid for **6a**, is surely not true for **6b**. However, an alternative assignment for the reduction pattern of this species has also to be taken into account. If the reduction potentials of peripheral and central  $-\text{N}=\text{C}$ -pyrazine- $\text{C}=\text{N}-$  units are close enough, the first reduction process at  $-0.42$  V could be a bi-electronic one, involving two closely spaced one-electron reductions involving the peripheral units. The second reduction at  $-0.56$  V would be the reduction of the central  $-\text{N}=\text{C}$ -pyrazine- $\text{C}=\text{N}-$  unit, displaced at more negative potential by the presence of two added electrons on the periphery. This third electron could be introduced in **6b** at mild potentials, differently from **6a** (see above), because the delocalization of the LUMO orbitals is reduced in **6b**. Within such a hypothesis, the inter-unit interaction would be responsible for the 140 mV shifting of the reduction of the

central  $-\text{N}=\text{C}-\text{pyrazine}-\text{C}=\text{N}-$  redox-active site compared to the reduction of the two peripheral almost identical sites. This could appear in contradiction with the splitting (100 mV) of the reduction potentials of the two  $-\text{N}=\text{C}-\text{pyrazine}-\text{C}=\text{N}-$  units in **4a** (see above), because the pyrazine-based “bridge” of **4a** should guarantee a better electronic interaction than the pyrimidine-based “bridges” of **6b**, but this apparent discrepancy is dispelled upon consideration that in **4a** the interaction involves only two redox-active centers and not three as in **6b**.

In summarizing the results obtained by the redox behavior, it is interesting to note that whereas the weak  $\beta$  value calculated from the oxidation potential data suggested that the molecular racks studied here can be considered as p-type molecular wires (see above and reference [17]), the delocalization suggested by the reduction potential of the hexanuclear **6a** indicates that these species can also behave as n-type molecular wires. A bifunctionality can therefore be proposed for the studied racks, and could be useful for their potential interest for implementation of supramolecular electronic devices.

### Absorption spectra

The absorption spectra of the  $\text{Ru}^{\text{II}}$  rack complexes show intense bands both in the UV and in the visible region (Table 2, Figure 11). A cursory look at the spectra shows three main regions in which dominant absorption bands are present: a) the wavelength region below 350 nm, with structured and intense bands; b) the  $360 < \lambda < 520$  nm region, containing a broad absorption, clearly comprising several components; and c) the  $520 < \lambda < 720$  nm region, dominated by an intense, structureless, and relatively narrow absorption

feature. A weak absorption tail is also present at wavelengths longer than 720 nm.

The bands in the  $\lambda < 360$  nm region are assigned to spin-allowed ligand-centered (LC) transitions, involving both the terpy ligands and the main bridging strands. The bands between 360 and 520 nm are assigned to lower-lying spin-allowed LC transitions involving the delocalized  $-\text{N}=\text{C}-\text{pyrazine}-\text{C}=\text{N}-$  units and (as far as the red side of the main absorption band is concerned, that is, for the absorption feature between 410 and 520 nm) to spin-allowed metal-to-ligand charge-transfer (MLCT) transitions, involving the terpyridine ligands and the  $-\text{N}-\text{pyrazine}-\text{N}-$  or  $-\text{N}-\text{pyrimidine}-\text{N}-$  bis-chelating moieties of the molecular strand. The band at wavelengths longer than 520 nm is assigned to spin-allowed MLCT transitions involving the  $-\text{N}=\text{C}-\text{pyrazine}-\text{C}=\text{N}-$  subunits. Such assignments are based on the absorption spectra of the free ligands of **2a-c**,<sup>[2a]</sup> which allowed the identification of LC bands involving the various subunits of the strand(s) and the redox behavior (see above), clarifying the reduction order of the various subunits.

The absorption spectra of the racks are mainly additive, with the molar absorptivity of each band increasing with the number of subunits having transitions contributing to the specific band present in the molecular frame. As evidenced by the redox properties, there are slight differences within this general view, with MLCT involving the same ligand unit but different metal centers (e.g., inner or outer with respect to the multinuclear rack structures) expected to occur at slightly different energies. However, such differences appear to be too small to be clearly evidenced in the absorption properties.

Finally, the features at low energy ( $\lambda > 720$  nm) are assigned to spin-forbidden MLCT transitions.

### Luminescence properties

All the rack-type compounds investigated here show luminescence both at room temperature in acetonitrile fluid solution and at 77 K in rigid matrix. Relevant data are collected in Table 2 and some spectra are shown in Figure 12. All the emissions are assigned to triplet MLCT states.

The dinuclear compound **2d** emits in the visible region, similar, under both experimental conditions (77 and 298 K), to the emissions of compound **2a**, formerly studied,<sup>[2a]</sup> and containing very similar subunits. For all the other species, emission occurs in the near-infrared region. For the already studied dinuclear species **2b** and **2c**, which contain the  $-\text{N}=\text{C}-\text{pyrazine}-\text{C}=\text{N}-$  or  $-\text{N}=\text{C}-\text{pyrimidine}-\text{C}=\text{N}-$  unit, it was suggested<sup>[2a]</sup> that an eventual emission could occur in the near-infrared region, because the lowest-energy spin-allowed MLCT absorption bands of these species lie at wavelengths longer than 600 nm and the energy difference between lowest-lying <sup>1</sup>MLCT absorption maxima and <sup>3</sup>MLCT emission maxima in  $\text{Ru}^{\text{II}}$  polypyridine complexes is typically  $5000-6000 \text{ cm}^{-1}$ .<sup>[18,24]</sup> The high-nuclearity racks studied here contain the  $-\text{N}=\text{C}-\text{pyrazine}-\text{C}=\text{N}-$  unit, responsible for the low-lying MLCT absorption band, and therefore near-IR

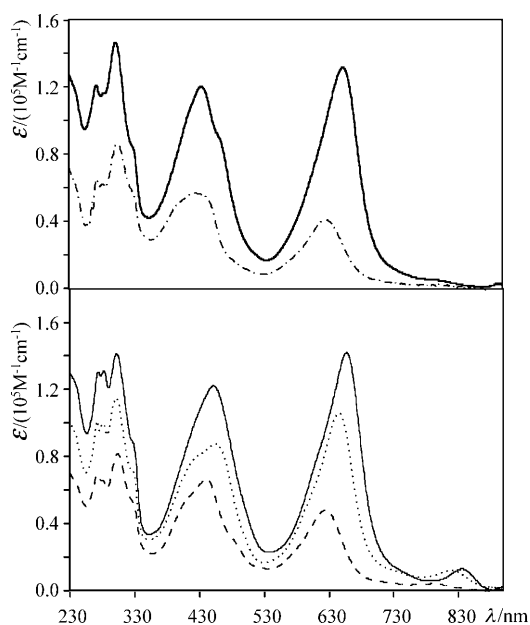


Figure 11. Absorption spectra of **3a** (---), **6a** (—), **4a** (.....), **3b** (-.-.-), **6b** (—).

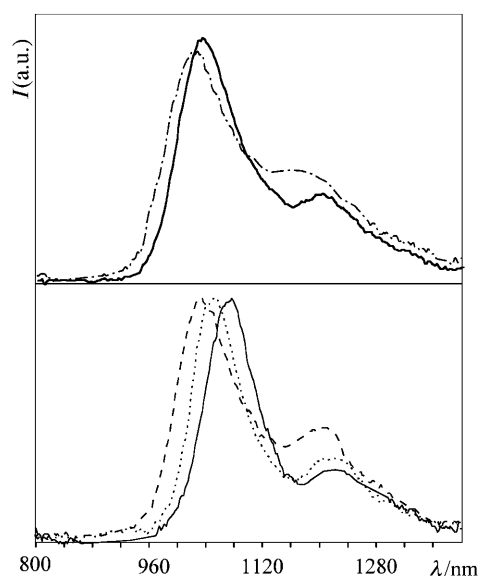


Figure 12. Emission spectra of **3a** (---), **6a** (—), **4a** (.....), **3b** (-·-·-), **6b** (—).

emissions could be inferred also for these species. However, it should be considered that Ru-based MLCT emissions in the near-infrared suffer from the effects of the energy-gap law,<sup>[25]</sup> which makes infrared MLCT emission quite rare, because of favorable Franck–Condon factors for radiationless decay. The inverted dependence of the rate constant for the radiative decay on emissive energy<sup>[26]</sup> further complicates the possibility of detecting MLCT emission in the near-infrared. As a consequence, reported examples of Ru-based MLCT emission spectra at wavelengths longer than 900 nm are extremely limited.<sup>[27]</sup>

In spite of the considerations mentioned above concerning difficulties in obtaining MLCT infrared emissions, all the Ru<sup>II</sup> racks studied here show MLCT emissions peaking at  $\lambda$  longer than 1000 nm (Table 2, Figure 12). The spectra also exhibit a net structural progression, even at room temperature, uncommonly found under these experimental conditions. To the best of our knowledge, this is a first time that a net, structured emission for Ru<sup>II</sup> complexes at wavelengths longer than 1000 nm has been reported, even at room temperature.<sup>[28,29]</sup>

A closer look at the energy differences among the emission spectra of the various species provides interesting hints. For example, the energy emission moves to lower energy in the series **3b**, **6b**, **3a**, **4a**, and **6a**. All the emissions are assigned to Ru-to-( $-\text{N}=\text{C}$ -pyrazine- $\text{C}=\text{N}-$  unit) CT triplet state(s). However, although the acceptor ligand of the MLCT emitting level is roughly identical in all the species, some slight differences exist, as shown by the reduction behavior. For example, the presence of multiple  $-\text{N}=\text{C}$ -pyrazine- $\text{C}=\text{N}-$  units allows for some delocalization, decreasing the energy of the MLCT state. This is reflected in the energy emission of **3a** (1040 nm), **4a** (1052 nm), and **6a** (1078 nm), in which the number of  $-\text{N}=\text{C}$ -pyrazine- $\text{C}=\text{N}-$  acceptor units increases from one to three. Moreover, the

presence, in the vicinity of a  $-\text{N}=\text{C}$ -pyrazine- $\text{C}=\text{N}-$  unit, of an  $-\text{N}$ -pyrazine- $\text{N}-$  moiety or of an  $-\text{N}$ -pyrimidine- $\text{N}-$  moiety has different effects: apparently, the former moiety contributes to the stabilization of the emitting MLCT level to a larger extent than the latter one (e.g., compare the emission of **6a** with that of **6b**, Table 2), most likely by increasing interaction between the bridging ligand moieties (see reduction). Therefore, the overall structure of the racks allows for fine tuning of the luminescence properties.

The net structure of the emission spectra of the compounds yields other interesting information: highly structured MLCT emission spectra are connected with relatively small Huang–Rhys coupling constants, that is, negligible displacements of excited-state nuclear coordinates relative to ground-state coordinates.<sup>[30]</sup> This suggests that the emitting MLCT states have geometries very similar to those of the ground state in the studied complexes, most likely as a consequence of the highly organized and rigid nature of the molecular racks. This is particularly shown in **4a** and **6a**, with a Huang–Rhys factor  $S$  (0.50 and 0.43), which is smaller relative to that of the other species [e.g.  $S$  values of **3a** and **3b** are 0.70 and 0.67, respectively; more details are given in the Supporting Information; for comparison, the factor  $S$  for  $[\text{Ru}(\text{bpy})_3]^{2+}$  (bpy = 2,2'-bipyridine) in the same experimental conditions approaches 1.0<sup>[32f]</sup>], and could be a further indication of significant electron delocalization in the MLCT acceptor ligand of these larger racks due to the presence of multiple  $-\text{N}=\text{C}$ -pyrazine- $\text{C}=\text{N}-$  units separated by pyrazine-based moieties. The similarity in ground- and excited-state structures of the rack compounds, as suggested by the emission spectra profiles, tends to reduce the rate constant of radiationless decay, and would be at the origin of the detectable emission in the near-infrared. Please also note that the indications suggested by the emission spectral profiles, as well as the energy difference in the emission spectra between the hexanuclear species mentioned above, strictly agree with the interpretation of the reduction data, in particular with the delocalized nature assigned to the LUMO of **6a**.

Unfortunately, information on excited-state lifetimes are not yet available (the lifetime was shorter than 2 ns, the time limit of our equipment), and quantum yield data are not known yet, owing to difficulties in finding reliable quantum yield standards in the infrared region, and therefore further discussion of the excited-state properties cannot be made. In particular, the lack of quantum yield data limits the discussion of possible applicative developments. Nevertheless, the conclusions derived from the analysis of the emission spectra profiles indirectly suggest that interesting quantum yield values could be obtained. In this context, one thinks of infrared emitters, the most often employed and promising systems for optical communication, for example, in short-range communication among computer peripherals and personal digital assistants. Infrared light with a wavelength between 1100 and 1700 nm, coupling least dispersion with best transmission properties, is the best choice for standard silica fibers.<sup>[34]</sup> Our results could therefore open new

and somewhat unexpected possibilities for MLCT emitters in the optical communication field.

## Conclusion

A series of new metal-containing molecular racks, spanning a nuclearity from two to six, was synthesized and the absorption spectra, redox behavior, and luminescence properties were investigated. The main results are summarized here:

The chemical diversity introduced in the structures by the isomeric possibilities offered by the hydrazone-based array led to interesting differences in the properties of the rack-type architectures. Further structural and functional diversities are offered by using pyrazine or pyrimidine subunits as moieties of the bridging molecular strand polytopic ligands.

In spite of the complexity of the molecular arrays, spectroscopic as well as redox processes can be assigned to specific subunits.

Oxidation behavior shows that non-negligible electronic interaction takes place between the peripheral metal centers, even in the larger species, thus indicating that the multimetallic systems can behave as efficient p-type “molecular wires”. Reduction processes show that the same species can behave as n-type “molecular wires”, particularly in the species containing pyrazine subunits in which some electron delocalization can take place within the larger molecular strands used as bridging ligand. The molecular racks can therefore be seen as bifunctional molecular wires.

Rather unusual room-temperature structured MLCT emissions in the near-infrared region take place for most of the complexes, a feature of potential interest for optical communication devices.

## Experimental Section

**Materials and general methods:** The following compounds were prepared as previously described: **21** (from **22**) and **26**,<sup>[6]</sup> **19**,<sup>[9]</sup> **18**,<sup>[10]</sup> **24**,<sup>[8]</sup> **14**,<sup>[12]</sup> **15**,<sup>[11]</sup> and [Ru(terpy)Cl<sub>3</sub>].<sup>[15]</sup> The following reagents were purchased from commercial sources: RuCl<sub>3</sub> (Aldrich, Avocado), terpy (Aldrich, Avocado), 2,5-dimethylpyrazine (Aldrich), benzaldehyde (Aldrich), benzoic anhydride (Aldrich). The 400 MHz <sup>1</sup>H and 100 MHz <sup>13</sup>C NMR spectra were recorded on a Bruker Ultrashield Avance 400 spectrometer and the 300 MHz <sup>1</sup>H and 75 MHz <sup>13</sup>C NMR spectra were recorded on a Bruker 300 spectrometer. The solvent residual signal was used as an internal reference for both <sup>1</sup>H (CD<sub>3</sub>CN, δ = 1.94 ppm; CDCl<sub>3</sub>, δ = 7.26 ppm) and <sup>13</sup>C NMR (CD<sub>3</sub>CN, δ = 118.26 ppm, CN group; CDCl<sub>3</sub>, δ = 77.00 ppm) spectra. The following notation is used for the <sup>1</sup>H NMR spectral splitting patterns: singlet (s), doublet (d), triplet (t), multiplet (m). The following 2D-NMR experiments were used: COSY, NOESY, and ROESY; they were carried out on 300 MHz or 500 MHz Bruker spectrometers. FAB-MS, EIMS, and ES-MS measurements were performed by the Service de Spectrométrie de Masse, Université Louis Pasteur. Melting points were recorded on a Büchi B-540 melting point apparatus and are uncorrected. Absorption spectra were recorded on a JASCO V570 spectrophotometer. For luminescence spectra at wavelengths shorter than 900 nm, a Jobin Yvon-Spex Fluoromax 2 spectrofluorimeter was used, equipped with a Hamamatsu R3896 photomultiplier, and the spectra were corrected for

photomultiplier response by using a program purchased with the fluorimeter. The emission spectra in the near-IR region were recorded on an Edinburgh FLS920 spectrofluorimeter, equipped with a liquid nitrogen cooled hyperpure germanium crystal as a detector. Luminescence lifetimes were determined by time-correlated single-photon-counting (TCSPC) with an Edinburgh OB900 spectrometer (light pulse: Hamamatsu PL2 laser diode, pulse width 59 ps at 408 nm; or nitrogen discharge, pulse width at 337 nm: 2 ns). Electrochemical measurements were carried out on samples in argon-purged acetonitrile at room temperature with a PAR273 multipurpose equipment interfaced to a PC. The working electrode was a glassy carbon (8 mm<sup>2</sup>, Amel) electrode. The counter electrode was a Pt wire, and the reference electrode was an SCE separated through a fine glass frit. The concentration of the samples was about 5 × 10<sup>-4</sup> M. Tetrabutylammonium hexafluorophosphate was used as supporting electrolyte and its concentration was 0.05 M. Cyclic voltammograms were obtained at scan rates of 20, 50, 200, and 500 mV s<sup>-1</sup>. For reversible processes, half-wave potentials (vs. SCE) were calculated as the average of the cathodic and anodic peaks. The criteria for reversibility were the separation of 60 mV between the cathodic and anodic peaks, the close to unity ratio of the intensities of the cathodic and anodic currents, and the constancy of the peak potential on changing scan rate. The number of exchanged electrons was measured with differential pulse voltammetry experiments performed with a scan rate of 20 mV s<sup>-1</sup>, a pulse height of 75 mV, and a duration of 40 ms, and by taking advantage of the presence of ferrocene used as the internal reference.

Experimental uncertainties are as follows: absorption maxima, 2 nm; molar absorption coefficient, 10%; emission maxima, 5 nm; excited state lifetimes, 10%; redox potentials, 10 mV.

The NMR assignments in the data below refer to formulae given in Schemes 1 and 2 and Figure 13.

### Synthesis

**[Ru(terpy)(7)][PF<sub>6</sub>]<sub>2</sub> (1):** An ethanol/water mixture (6 mL, 1:1 v/v) was added to [Ru(terpy)Cl<sub>3</sub>] (23 mg, 0.052 mmol, 1.36 equiv) and free ligand **7** (8 mg, 0.038 mmol, 1 equiv). The mixture was heated under reflux for 19 h, then cooled to room temperature and filtered. Excess aqueous NH<sub>4</sub>PF<sub>6</sub> was added to the solution and the precipitate was collected. The solid was purified by recrystallization from acetonitrile/CHCl<sub>3</sub> to afford **1** (16 mg, ≈51%). Brown solid; m.p. >300°C; <sup>1</sup>H NMR (300 MHz, CD<sub>3</sub>CN): δ = 8.79 (s, 1H), 8.69 (s, 1H), 8.66 (s, 1H), 8.47 (ddd, *J* = 0.7, 1.3, 8.2 Hz, 1H), 8.37 (dd, *J* = 7.9, 8.4 Hz, 1H), 8.21 (ddd, *J* = 0.8, 1.5, 5.5 Hz, 1H), 7.9 (td, *J* = 1.5, 6.2 Hz, 1H), 7.79–7.73 (m, 1H), 7.69–7.60 (m, 2H), 7.37 (ddd, *J* = 1.3, 5.5, 6.9 Hz, 1H), 7.14 (d, *J* = 8.8 Hz, 1H), 6.98–6.94 (m, 1H), 6.89 (ddd, *J* = 1.5, 5.5, 7.3 Hz, 1H), 6.77 (ddd, *J* = 0.7, 1.6, 5.7 Hz, 1H), 6.59 ppm (ddd, *J* = 1.1, 5.7, 6.8 Hz, 1H); <sup>13</sup>C NMR (75 MHz, CD<sub>3</sub>CN): δ = 161.07, 159.70, 158.60, 156.18, 153.69, 152.52, 150.83, 140.96, 139.24, 138.69, 137.16, 136.57, 128.57, 126.68, 126.59, 125.39, 124.53, 120.37, 110.34, 35.45 ppm; HRMS (ES): *m/z*: calcd for C<sub>12</sub>H<sub>12</sub>N<sub>4</sub>C<sub>15</sub>H<sub>11</sub>N<sub>3</sub>-Ru-PF<sub>6</sub><sup>+</sup>: 692.0702 [M-PF<sub>6</sub>]<sup>+</sup>; found: 692.0692.

**[[Ru(terpy)<sub>2</sub>(8)][PF<sub>6</sub>]<sub>4</sub> (2d):** An ethanol/water mixture (1:1, v/v; 6 mL) was added to [Ru(terpy)Cl<sub>3</sub>] (22 mg, 0.05 mmol, 2.5 equiv) and free ligand **8** (7 mg, 0.02 mmol, 1 equiv). The mixture was heated under reflux for 19 h, then cooled to room temperature and filtered. Excess aqueous NH<sub>4</sub>PF<sub>6</sub> was added to the solution and the precipitate was collected. The solid was purified by recrystallization from acetonitrile/CHCl<sub>3</sub> to afford **2d** (20 mg, 62%). Brown solid; m.p. >300°C; <sup>1</sup>H NMR (300 MHz, CD<sub>3</sub>CN): δ = 8.71 (d, *J* = 8.1 Hz, 4H; T<sub>3</sub>), 8.53 (s, 2H; U), 8.51–8.41 (m, 6H; T<sub>4</sub>+T<sub>6</sub>), 8.04–7.96 (m, 8H; T<sub>1</sub>+T<sub>3</sub>), 7.67–7.60 (m, 4H; P+Q), 7.31 (ddd, *J* = 1.3, 5.7, 7.1, 4H; T<sub>2</sub>), 6.88 (ddd, *J* = 2.3, 5.7, 6.8 Hz, 2H; R), 6.78–6.74 (m, 2H; S), 6.38 (s, 2H; K), 3.61 ppm (s, 6H; J); <sup>13</sup>C NMR (75 MHz, CD<sub>3</sub>CN): δ = 160.51, 158.66, 156.25, 153.90, 152.53, 152.01, 139.76, 139.35, 138.16, 137.76, 130.53, 128.50, 127.07, 126.93, 125.67, 125.03, 35.68 ppm; MS (ES): *m/z*: calcd for C<sub>18</sub>H<sub>18</sub>N<sub>8</sub>2C<sub>15</sub>H<sub>11</sub>N<sub>3</sub>2Ru-3PF<sub>6</sub><sup>+</sup>: 1451.0591 [M-3PF<sub>6</sub>]<sup>+</sup>; found: 1451.0815; *m/z*: calcd for C<sub>18</sub>H<sub>18</sub>N<sub>8</sub>2C<sub>15</sub>H<sub>11</sub>N<sub>3</sub>2Ru-PF<sub>6</sub><sup>3+</sup>: 387.0432 [M-3PF<sub>6</sub>]<sup>3+</sup>; found: 387.0543.

**[[Ru(terpy)<sub>3</sub>(9a)][PF<sub>6</sub>]<sub>6</sub> (3a):** An ethanol/water mixture (1:1, v/v; 6 mL) was added to [Ru(terpy)Cl<sub>3</sub>] (23.6 mg, 0.054 mmol, 3.6 equiv) and free ligand **9a** (7.2 mg, 0.015 mmol, 1 equiv). The mixture was heated under

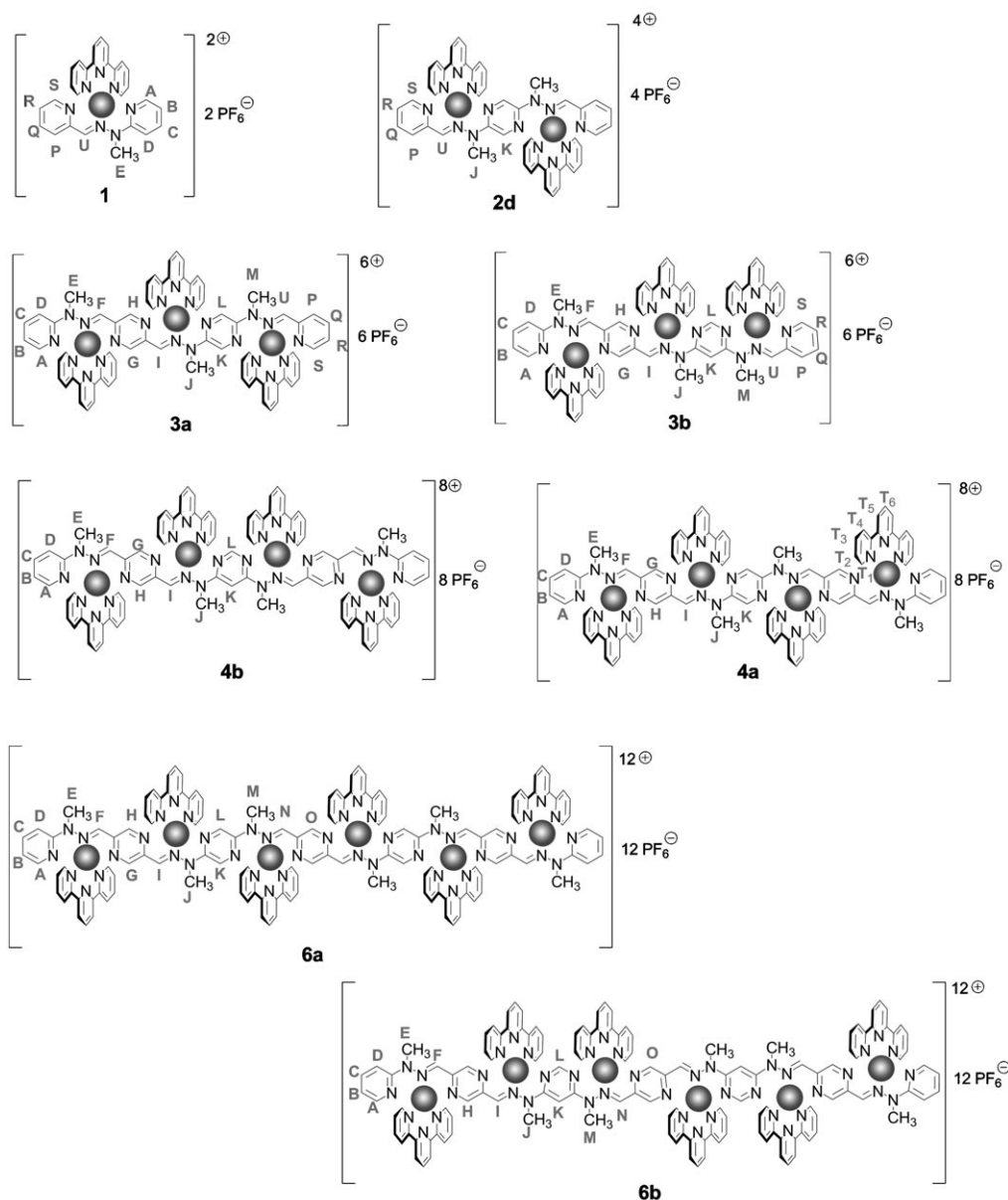


Figure 13. Structural formulae of new complexes **1**, **2d**, **3a,b**, **4a,b**, and **6a,b** and identification of NMR sites.

reflux for 19 h, then cooled to room temperature and filtered. Excess aqueous  $\text{NH}_4\text{PF}_6$  was added to the solution and the precipitate was collected. The solid was purified by recrystallization from acetonitrile/ $\text{CHCl}_3$  to afford **3a** (23 mg,  $\approx 65\%$ ). Green solid; m.p.  $> 300^\circ\text{C}$ ;  $^1\text{H}$  NMR (300 MHz,  $\text{CD}_3\text{CN}$ ):  $\delta = 8.76$  (d,  $J = 8.1$  Hz, 2H; 1T<sub>3</sub>), 8.67 (d,  $J = 8.3$  Hz, 2H; 1T<sub>3</sub>), 8.66 (d,  $J = 8.3$  Hz, 2H; 1T<sub>3</sub>), 8.60–8.30 (m, 9H; 3T<sub>4</sub>+3T<sub>6</sub>), 8.51 (s, 1H; U), 8.26 (s, 1H; F), 8.07 (s, 1H; I), 8.03–7.90 (m, 8H; 3T<sub>3</sub>+1T<sub>1</sub>), 7.85 (dd,  $J = 0.8, 5.5$  Hz, 2H; 1T<sub>1</sub>), 7.72 (d,  $J = 5.1$  Hz, 2H; 1T<sub>1</sub>), 7.68–7.61 (m, 3H; C+P+Q), 7.30–7.11 (m, 7H; D+3T<sub>2</sub>), 7.03 (s, 1H; H), 6.90–6.84 (m, 2H; G+R), 6.78–6.73 (m, 2H; A+S), 6.65–6.59 (m, 1H; B), 6.361 (s, 1H; K), 6.356 (s, 1H; L), 3.95 (s, 3H; E), 3.60 (s, 3H; M), 3.48 ppm (s, 3H; J);  $^{13}\text{C}$  NMR (75 MHz,  $\text{CD}_3\text{CN}$ ):  $\delta = 158.18, 157.60, 156.44, 156.19, 155.76, 155.44, 154.84, 154.65, 153.81, 153.19, 152.04, 151.68, 150.76, 146.57, 145.76, 141.91, 140.18, 139.92, 139.79, 139.47, 139.42, 138.83, 138.22, 133.80, 132.91, 131.32, 130.27, 128.52, 128.46, 127.20, 127.07, 125.80, 125.71, 125.58, 125.45, 125.02, 121.49, 111.01, 35.86, 35.73$  ppm.

**[[Ru(terpy)<sub>3</sub>(9b)][PF<sub>6</sub>]<sub>6</sub> (3b)**: An ethanol/water mixture (1:1, v/v; 5 mL) was added to  $[\text{Ru}(\text{terpy})\text{Cl}_3]$  (21 mg, 0.048 mmol, 3.2 equiv) and free ligand **9b** (7.2 mg, 0.015 mmol, 1 equiv). The mixture was heated under reflux for 19 h, then cooled to room temperature and filtered. Excess aqueous  $\text{NH}_4\text{PF}_6$  was added to the solution and the precipitate was collected. The solid was purified by recrystallization from acetonitrile/ $\text{CHCl}_3$  to afford **3b** (24 mg, 68%). Green solid; m.p.  $> 300^\circ\text{C}$ ;  $^1\text{H}$  NMR (400 MHz,  $\text{CD}_3\text{CN}$ ):  $\delta = 8.91$  (s, 1H), 8.70 (d,  $J = 8.2$  Hz, 2H), 8.59 (d,  $J = 7.8$  Hz, 2H), 8.51–8.42 (m, 7H), 8.35–8.25 (m, 5H), 8.22 (s, 1H), 7.98–7.79 (m, 9H), 7.69–7.63 (m, 2H), 7.60–7.56 (m, 2H), 7.25–7.07 (m, 11H), 6.93–6.89 (m, 2H), 6.79–6.76 (m, 1H), 6.67–6.62 (m, 1H), 6.47 (s, 1H), 5.04 (s, 1H), 4.13 (s, 3H), 4.00 (s, 3H), 3.95 ppm (s, 3H);  $^{13}\text{C}$  NMR (75 MHz,  $\text{CD}_3\text{CN}$ ):  $\delta = 163.90, 163.03, 159.83, 159.21, 158.38, 158.19, 157.93, 157.70, 155.96, 155.77, 155.47, 155.44, 155.43, 154.80, 154.69, 153.91, 152.89, 150.76, 148.00, 146.60, 141.95, 141.85, 140.18, 139.95, 139.61, 139.54, 138.95, 138.85, 138.23, 137.58, 132.59, 128.66, 128.63, 128.57, 128.48, 127.84, 125.63, 125.29, 125.16, 125.08, 124.62, 124.07,$

121.70, 111.16, 88.79, 35.81, 35.62, 35.53 ppm; HRMS (ES):  $m/z$ : calcd for  $C_{60}H_{57}F_{18}N_{21}P_3Ru_3^{3+}$ : 639.706  $[M-3PF_6]^{3+}$ ; found: 639.706.

**[[Ru(terpy)]<sub>4</sub>(10a)][PF<sub>6</sub>]<sub>8</sub> (4a)**: An ethanol/water mixture (1:1, v/v; 7 mL) was added to [Ru(terpy)Cl<sub>3</sub>] (25 mg, 0.057 mmol, 4.8 equiv) and free ligand **10a** (7.3 mg, 0.012 mmol, 1 equiv). The mixture was heated under reflux for 19 h, then cooled to room temperature and filtered. Excess aqueous NH<sub>4</sub>PF<sub>6</sub> was added to the solution and the precipitate was collected. The solid was purified by recrystallization from acetonitrile/CHCl<sub>3</sub> to afford **4a** (21 mg, ≈57%). Green solid; m.p. >300 °C; <sup>1</sup>H NMR (300 MHz, CD<sub>3</sub>CN): δ=8.72 (d,  $J$ =7.9 Hz, 4H; 1T<sub>3</sub>), 8.67 (d,  $J$ =8.1 Hz, 4H; 1T<sub>3</sub>), 8.56–8.38 (m, 12H; 2T<sub>6</sub>+2T<sub>4</sub>), 8.27 (s, 2H; F), 8.07 (s, 2H; I), 8.00–7.89 (m, 8H; 2T<sub>3</sub>), 7.85 (dd,  $J$ =0.7, 5.7 Hz, 4H; 1T<sub>1</sub>), 7.68 (dd,  $J$ =0.8, 5.5 Hz, 4H; 1T<sub>1</sub>), 7.64 (ddd,  $J$ =1.7, 7.4, 8.9 Hz, 2H; C), 7.22 (ddd,  $J$ =1.1, 5.5, 7.5 Hz, 4H; 1T<sub>2</sub>), 7.20–7.10 (m, 6H; 1T<sub>2</sub>+D), 7.05 (d,  $J$ =0.7 Hz, 2H; H), 6.87 (d,  $J$ =0.7 Hz, 2H; G), 6.77–6.73 (m, 2H; A), 6.64–6.59 (m, 2H; B), 6.35 (s, 2H; K), 3.94 (s, 6H; E), 3.48 ppm (s, 6H; J); <sup>13</sup>C NMR (75 MHz, CD<sub>3</sub>CN): δ=159.21, 158.30, 158.16, 157.76, 156.27, 155.71, 155.41, 154.74, 154.65, 152.33, 150.74, 146.71, 145.76, 141.91, 140.21, 139.92, 139.51, 138.85, 134.31, 132.92, 131.07, 128.53, 128.48, 125.84, 125.60, 125.43, 125.04, 121.51, 111.04, 35.95, 35.76 ppm; HRMS (ES):  $m/z$ : calcd for  $C_{30}H_{30}N_{16}^+4C_{15}H_{11}N_3^+4Ru\ 5PF_6^{3+}$ : 892.7024  $[M-3PF_6]^{3+}$ ; found: 892.7197.

**[[Ru(terpy)]<sub>4</sub>(10b)][PF<sub>6</sub>]<sub>8</sub> (4b)**: An ethanol/water mixture (1:1, v/v; 6 mL) was added to [Ru(terpy)Cl<sub>3</sub>] (23 mg, 0.052 mmol, 4.3 equiv) and free ligand **10b** (7.2 mg, 0.012 mmol, 1 equiv). The mixture was heated under reflux for 19 h, then cooled to room temperature and filtered. Excess aqueous NH<sub>4</sub>PF<sub>6</sub> was added to the solution and the precipitate was collected. The solid was purified by recrystallization from acetonitrile/CHCl<sub>3</sub> to afford **4b** (24 mg, ≈66%). Green solid; m.p. >300 °C; <sup>1</sup>H NMR (400 MHz, CD<sub>3</sub>CN): δ=8.69 (d,  $J$ =8.3 Hz, 4H), 8.56 (d,  $J$ =8.3 Hz, 4H), 8.50–8.40 (m, 10H), 8.29 (d,  $J$ =7.9, 4H), 8.22 (s, 2H), 7.98–7.80 (m, 12H), 7.64 (t,  $J$ =7.9 Hz, 2H), 7.55 (d,  $J$ =5.4 Hz, 4H), 7.25–7.17 (m, 6H), 7.17 (d,  $J$ =8.3 Hz, 2H), 7.10–7.04 (m, 6H), 6.76 (d,  $J$ =5.4 Hz, 2H), 6.63 (t,  $J$ =6.6 Hz, 2H), 6.48 (s, 1H), 5.08 (s, 1H), 3.98 (s, 6H), 3.94 ppm (s, 6H); <sup>13</sup>C NMR (75 MHz, CD<sub>3</sub>CN): δ=163.41, 159.17, 158.16, 157.63, 155.62, 155.44, 155.40, 154.79, 154.68, 150.73, 148.13, 146.56, 141.93, 140.16, 139.93, 139.51, 138.99, 138.95, 138.01, 132.58, 128.64, 128.54, 125.61, 125.27, 125.07, 124.70, 121.70, 111.15, 89.35, 35.81, 35.66 ppm; MS (ES):  $m/z$ : calcd for  $C_{30}H_{30}N_{16}^+4C_{15}H_{11}N_3^+4Ru\ 6PF_6^{2+}$ : 1411.036  $[M-2PF_6]^{2+}$ ; found: 1411.048.

**Precursor 5**: A solution of **17** (50 mg, 0.297 mmol, 2.23 equiv) in EtOH (30 mL) was added to a solution of **13** (32 mg, 0.133 mmol, 1 equiv) in EtOH (250 mL). The mixture was stirred overnight at room temperature. Then the solution was concentrated to 20 mL, and filtered, and the precipitate was washed with EtOH and dried under vacuum for 10 h to afford **5** (27 mg, 52%). Yellow solid; <sup>1</sup>H NMR (300 MHz, CDCl<sub>3</sub>): δ=9.14 (d,  $J$ =1.3 Hz, 1H), 9.12 (d,  $J$ =1.3 Hz, 1H), 8.63 (d,  $J$ =1.7 Hz, 1H), 8.26 (ddd,  $J$ =0.8, 1.9, 4.9 Hz, 1H), 8.17 (d,  $J$ =1.5 Hz, 1H), 7.78–7.62 (m, 4H), 6.87 (ddd,  $J$ =1.1, 5.1, 7 Hz, 1H), 3.73 (d,  $J$ =0.8 Hz, 3H), 3.64 (d,  $J$ =0.8, 3H), 3.27 ppm (s, 3H); <sup>13</sup>C NMR (75 MHz, CDCl<sub>3</sub>): δ=157.15, 153.36, 148.58, 148.14, 147.04, 146.06, 140.63, 140.53, 137.75, 132.22, 131.04, 129.76, 127.05, 116.63, 110.21, 41.98, 30.14, 20.70 ppm; HRMS (ES):  $m/z$ : calcd for  $C_{18}H_{21}N_{11}Na^+$ : 414.187  $[M+Na]^+$ ; found: 414.191.

**[[Ru(terpy)]<sub>6</sub>(12a)][PF<sub>6</sub>]<sub>12</sub> (6a)**: An ethanol/water mixture (1:1, v/v; 5 mL) was added to [Ru(terpy)Cl<sub>3</sub>] (25 mg, 0.057 mmol, 7.1 equiv) and free ligand **12a** (7 mg, 0.008 mmol, 1 equiv). The mixture was heated under reflux for 19 h, then cooled to room temperature and filtered. Excess aqueous NH<sub>4</sub>PF<sub>6</sub> was added to the solution and the precipitate was collected. The solid was purified by recrystallization from acetonitrile/CHCl<sub>3</sub> to afford **6a** (16 mg, ≈51%). Green solid; m.p. >300 °C; <sup>1</sup>H NMR (300 MHz, CD<sub>3</sub>CN): δ=8.71 (d,  $J$ =8.2 Hz, 4H; 1T<sub>3</sub>), 8.65 (d,  $J$ =8.2 Hz, 8H; 2T<sub>3</sub>), 8.55–8.35 (m, 18H; 3T<sub>6</sub>+3T<sub>4</sub>), 8.24 (s, 2H; F), 8.03 (s, 2H; I), 8.01 (s, 2H; N), 7.97–7.88 (m, 12H; 3T<sub>3</sub>), 7.83 (dd,  $J$ =0.6, 5.6 Hz, 4H; 1T<sub>1</sub>), 7.69–7.58 (m, 10H; C+2T<sub>1</sub>), 7.21 (ddd,  $J$ =1.2, 5.6, 7 Hz, 4H; 1T<sub>2</sub>), 7.15–7.05 (m, 10H; D+2T<sub>2</sub>), 7.02 (s, 2H; H), 6.84 (s, 2H; G), 6.74 (dd,  $J$ =1.2, 5.6 Hz, 2H; A), 6.72 (s, 2H; O), 6.64–6.59 (m, 2H; B), 6.335 and 6.328 (s, 2H+2H; K+L), 3.93 (s, 6H; E), 3.44 ppm (s, 12H; J+M); <sup>13</sup>C NMR (75 MHz, CD<sub>3</sub>CN): δ=158.20, 158.16, 157.79,

156.77, 156.26, 155.71, 155.56, 155.40, 154.78, 154.73, 154.65, 152.42, 152.20, 150.74, 146.75, 146.02, 145.77, 141.93, 140.21, 139.92, 139.58, 139.51, 138.85, 134.39, 132.91, 131.17, 131.10, 128.53, 128.47, 128.43, 125.83, 125.58, 125.42, 125.02, 121.52, 111.03, 35.98, 35.90, 35.75 ppm; MS (ES):  $m/z$ : calcd for  $C_{42}H_{42}N_{24}^+6C_{15}H_{11}N_3^+6Ru\ 9PF_6^{3+}$ : 1398.028  $[M-3PF_6]^{3+}$ ; found: 1398.037; elemental analysis calcd (%) for **6a**·18H<sub>2</sub>O: C 32.01, H 2.93, N 11.88; found: C 31.75, H 2.93, N 11.95.

**[[Ru(terpy)]<sub>6</sub>(12b)][PF<sub>6</sub>]<sub>12</sub> (6b)**: An ethanol/water mixture (1:1, v/v; 5 mL) was added to [Ru(terpy)Cl<sub>3</sub>] (25 mg, 0.057 mmol, 7.1 equiv) and free ligand **12b** (7 mg, 0.008 mmol, 1 equiv). The mixture was heated under reflux for 19 h, then cooled to room temperature and filtered. Excess aqueous NH<sub>4</sub>PF<sub>6</sub> was added to the solution and the precipitate was collected. The solid was purified by recrystallization from acetonitrile/CHCl<sub>3</sub> to afford **6b** (12 mg, 38%). Green solid; m.p. >300 °C; <sup>1</sup>H NMR (400 MHz, CD<sub>3</sub>CN): δ=8.69 (d,  $J$ =8.3 Hz, 4H), 8.54 (d,  $J$ =7.84, 8H), 8.50–8.40 (m, 12H), 8.38 (s, 2H), 8.30–8.25 (m, 8H), 8.22 (s, 2H), 7.93 (t,  $J$ =7.9 Hz, 4H), 7.98–7.78 (m, 12H), 7.64 (t,  $J$ =7 Hz, 2H), 7.54 (d,  $J$ =5.4 Hz, 4H), 7.47 (d,  $J$ =5 Hz, 4H), 7.24–7.10 (m, 10H), 7.08–6.97 (m, 10H), 6.76 (d,  $J$ =5.8 Hz, 2H), 6.63 (t,  $J$ =6.2 Hz, 2H), 6.49 (s, 2H), 5.07 (s, 2H), 3.98 (s, 6H), 3.96 (s, 6H), 3.94 ppm (s, 6H).

**Pyridine-2-carboxaldehyde (pyrazine-2,5-diyl)dihydrazone (8)**: A solution of **17** (10 mg, 0.059 mmol, 1 equiv) and **25** (19.1 mg, 3 equiv) in EtOH (5 mL) was heated to reflux for 3 h. Then the mixture was cooled and filtered. The precipitate was washed with EtOH and dried for 10 h under high vacuum; this gave **8** (16 mg, ≈78%). Yellow solid; <sup>1</sup>H NMR (400 MHz, CDCl<sub>3</sub>): δ=8.69 (s, 2H), 8.56 (ddd,  $J$ =0.9, 1.4, 4.6 Hz, 2H), 8.01 (d,  $J$ =8.2 Hz, 2H), 7.74 (s, 2H), 7.70 (td,  $J$ =1.8, 7.9 Hz, 2H), 7.19 (ddd,  $J$ =1.2, 5, 7.3 Hz, 2H), 3.66 ppm (s, 6H); <sup>13</sup>C NMR (100 MHz, CDCl<sub>3</sub>): δ=155.25, 149.22, 148.13, 136.31, 134.57, 128.97, 122.45, 119.18, 29.90 ppm; HRMS (ES):  $m/z$ : calcd for  $C_{18}H_{18}N_8+Li^+$ : 353.1809  $[M+Li]^+$ ; found: 353.1809.

**Pyrazine-2,5-dicarboxaldehyde methyl[5-[1-methyl-2-(pyridin-2-ylmethyl)hydrazino]pyrazin-2-yl]hydrazone methyl(pyridin-2-yl)hydrazone (9a)**: A solution of **5** (15 mg, 0.038 mmol, 1 equiv) and **25** (5 mg, 1.2 equiv) in CHCl<sub>3</sub> (10 mL) was heated overnight at reflux. Then the solution was concentrated to 2 mL, and filtered, and the precipitate was washed with CHCl<sub>3</sub> and EtOH and dried under vacuum for 10 h to afford **9a** (10 mg, 54%) as a yellow solid. Its low solubility did not allow the recording of NMR spectra. HRMS (ES):  $m/z$ : calcd for  $C_{24}H_{24}N_{12}Li^+$ : 487.2402  $[M+Li]^+$ ; found: 487.2391.

**Pyrazine-2,5-dicarboxaldehyde methyl[6-[1-methyl-2-(pyridin-2-ylmethyl)hydrazino]pyrimidin-4-yl]hydrazone methyl(pyridin-2-yl)hydrazone (9b)**: A solution of **13** (10 mg, 0.041 mmol, 1 equiv) and **26** (11 mg, 1 equiv) in ethanol (30 mL) was heated overnight at reflux. Then the solution was concentrated to 15 mL, and filtered, and the precipitate was washed with EtOH and dried under vacuum for 10 h to afford **9b** (15 mg, 75%). Yellow solid; <sup>1</sup>H NMR (300 MHz, CDCl<sub>3</sub>): δ=9.33 (d,  $J$ =1.3 Hz, 1H), 9.20 (d,  $J$ =1.3 Hz, 1H), 8.62 (ddd,  $J$ =0.8, 1.7, 4.9 Hz, 1H), 8.48 (d,  $J$ =0.9, 1H), 8.28 (ddd,  $J$ =0.8, 1.9, 4.9 Hz, 1H), 8.23 (dt,  $J$ =0.9, 8.1 Hz, 1H), 8.01–7.94 (m, 2H), 7.88 (s, 1H), 7.85 (s, 1H), 7.80–7.75 (m, 2H), 7.67 (ddd,  $J$ =1.9, 7.1, 8.9 Hz, 1H), 7.28 (ddd,  $J$ =1.1, 4.9, 7.5 Hz, 1H), 6.89 (ddd,  $J$ =1.1, 4.9, 7 Hz), 3.77 (d,  $J$ =0.8, 3H), 3.72 (d,  $J$ =0.6 Hz, 3H), 3.70 ppm (d,  $J$ =0.6 Hz, 3H); <sup>13</sup>C NMR (75 MHz, CDCl<sub>3</sub>): δ=162.91, 162.53, 157.09, 156.88, 154.88, 149.33, 149.21, 147.96, 147.10, 141.13, 140.75, 137.80, 137.20, 136.89, 134.64, 131.98, 123.22, 119.76, 116.83, 110.24, 89.10, 29.81, 29.64, 29.58 ppm; HRMS (ES):  $m/z$ : calcd for  $C_{24}H_{24}N_{12}+H^+$ : 481.2320  $[M+H]^+$ ; found: 481.2314.

**Pyrazine-2,5-dicarboxaldehyde 2,2'-bis[methyl(pyridin-2-yl)hydrazone] 5,5'-[(pyrazine-2,5-diyl)bis(methylhydrazone)] (10a)**: A solution of **25** (29 mg, 0.120 mmol, 2 equiv) and **17** (10 mg, 1 equiv) in CHCl<sub>3</sub> (30 mL) was heated overnight at reflux. Then the solution was concentrated to 15 mL, and filtered, and the precipitate was washed with CHCl<sub>3</sub> and dried under vacuum for 10 h to afford **10a** (35 mg, ≈96%) as a yellow solid. Its low solubility did not allow the recording of NMR spectra.

**Pyrazine-2,5-dicarboxaldehyde 2,2'-bis[methyl(pyridin-2-yl)hydrazone] 5,5'-[(pyrimidine-4,6-diyl)bis(methylhydrazone)] (10b)**: A solution of **25** (20 mg, 0.083 mmol, 2 equiv) and **21** (7 mg, 1 equiv) in ethanol (30 mL) was heated overnight at reflux. Then the solution was concentrated to

15 mL, and filtered, and the precipitate was washed with EtOH and dried under vacuum for 10 h to afford **10b** (20 mg,  $\approx 78\%$ ). Its low solubility did not allow the recording of NMR spectra. Yellow solid; MS (ES):  $m/z$ : calcd for  $C_{30}H_{30}N_{16} + H^+$ : 615.2912  $[M+H]^+$ ; found: 615.2914.

**Precursor 11**: A solution of **21** (70 mg, 0.417 mmol, 2 equiv) in EtOH (30 mL) was added to a solution of **13** (50 mg, 0.207 mmol, 1 equiv) in EtOH (250 mL). The mixture was stirred overnight at room temperature. Then the solution was concentrated to 20 mL, and filtered, and the precipitate was washed with EtOH and dried under vacuum for 10 h to afford **11** (50 mg,  $\approx 62\%$ ). Yellow solid;  $^1H$  NMR (300 MHz,  $CDCl_3$ ):  $\delta = 9.20$  (d,  $J = 1.5$  Hz, 1H), 9.17 (d,  $J = 1.5$  Hz, 1H), 8.35 (d, 0.9 Hz, 1H), 8.27 (ddd,  $J = 0.9, 1.9, 4.9$  Hz, 1H), 7.80 (s, 1H), 7.76 (dt,  $J = 1, 8.7$  Hz, 1H), 7.72 (s, 1H), 7.66 (ddd,  $J = 1.9, 7, 8.9$  Hz, 1H), 7.07 (d,  $J = 0.9$  Hz, 1H), 6.88 (ddd,  $J = 1.1, 4.9, 7$  Hz, 1H), 4.12 (s, br, 2H), 3.73 (d,  $J = 0.6$  Hz, 3H), 3.68 (d,  $J = 0.6$  Hz, 3H), 3.67 ppm (s, 3H);  $^{13}C$  NMR (75 MHz,  $CDCl_3$ ):  $\delta = 164.95, 162.02, 157.05, 156.90, 148.93, 147.96, 147.08, 140.95, 140.83, 137.80, 134.18, 131.80, 116.84, 110.26, 84.96, 39.96, 29.77, 29.74$  ppm; HRMS (ES):  $m/z$ : calcd for  $C_{18}H_{22}N_{11} + H^+$ : 392.2054  $[M+H]^+$ ; found: 392.2043.

**Ligand 12a**: A solution of **5** (22 mg, 0.056 mmol, 1 equiv) and **14** (3.8 mg, 0.023 mmol, 0.4 equiv) in  $CHCl_3$  (30 mL) was heated overnight at reflux. Then the solution was concentrated to 15 mL, and filtered, and the precipitate was washed with  $CHCl_3$  and dried under vacuum for 10 h to afford **12a** (22 mg,  $\approx 55\%$ ). Its low solubility did not allow the recording of NMR spectra. Yellow solid; HRMS (ES):  $m/z$ : calcd for  $C_{42}H_{42}LiN_{24}^+$ : 889.418  $[M+Li]^+$ ; found: 889.421.

**Ligand 12b**: A solution of **11** (30 mg, 0.077 mmol, 2 equiv) and **14** (5 mg, 0.037 mmol, 1 equiv) in  $CHCl_3$  (30 mL) was heated overnight at reflux. Then the solution was concentrated to 15 mL, and filtered, and the precipitate was washed with  $CHCl_3$  and dried under vacuum for 10 h to afford **12b** (23 mg,  $\approx 44\%$ ). Its low solubility did not allow the recording of NMR spectra. Yellow solid; MS (ES):  $m/z$ : calcd for  $C_{42}H_{42}N_{24} + H^+$ : 883.4097  $[M+H]^+$ ; found: 883.4056; calcd for  $C_{42}H_{42}N_{24} + Na^+$ : 905.3916  $[M+Na]^+$ ; found: 905.3896.

**Pyrazine-2,5-dicarboxaldehyde methyl(pyridin-2-yl)hydrazone (13)**: A solution of **24** (130 mg, 1.057 mmol, 0.96 equiv) in EtOH (30 mL) was added to a solution of **14** (150 mg, 1.103 mmol, 1 equiv) in EtOH (250 mL). The mixture was stirred overnight at room temperature. Then the solution was concentrated to 30 mL and filtered. The solvent of the filtrate was evaporated under vacuum and the solid thus obtained was purified by flash chromatography ( $Al_2O_3$ ,  $CHCl_3$ /pentane 8:2) to afford **13** (100 mg, 0.415 mmol, 43%). Yellow solid;  $^1H$  NMR (400 MHz,  $CD_2CN$ ):  $\delta = 10.15$  (s, 1H), 9.38 (d,  $J = 1.8$  Hz, 1H), 9.06 (d,  $J = 1.2$  Hz, 1H), 8.31–8.28 (m, 1H), 7.78–7.75 (m, 1H), 7.74 (s, 1H), 7.70 (ddd,  $J = 1.8, 6.7, 8.5$  Hz, 1H), 6.97–6.92 (m, 1H), 3.76 ppm (s, 3H);  $^{13}C$  NMR (75 MHz,  $CDCl_3$ ):  $\delta = 192.12, 156.67, 154.09, 147.21, 144.46, 143.01, 141.81, 137.98, 130.79, 117.70, 110.55, 30.12$  ppm; MS (ES):  $m/z$ : calcd for  $C_{12}H_{12}N_5O + H^+$ : 242.1036  $[M+H]^+$ ; found: 242.1048.

**2,5-Bis(1-methylhydrazino)pyrazine (17)**: Under magnetic stirring, **18** (300 mg) was slowly added in portions to ice-cooled methylhydrazine (3 mL). The mixture was heated to reflux for 4 days under argon. After cooling of the mixture, methylhydrazine was evaporated,  $K_2CO_3$  (0.3 g) and  $CHCl_3$  (40 mL) were added to the solid residue, and the mixture was stirred for 10 min. The liquid phase was filtered. The solid–liquid extraction procedure was repeated 3 times with  $CHCl_3$  (without adding more  $K_2CO_3$ ), and the combined liquid fraction was evaporated. Filtration on alumina ( $CHCl_3$ ), followed by partial evaporation and precipitation with diethyl ether afforded **17** (50 mg, 23%). Brown solid, air-unstable;  $^1H$  NMR (400 MHz,  $CDCl_3$ ):  $\delta = 8.09$  (s, 2H), 3.88 (brs, 4H), 3.18 ppm (s, 6H);  $^{13}C$  NMR (100 MHz,  $CDCl_3$ ):  $\delta = 142.84, 131.95, 40.75$  ppm; MS (ES):  $m/z$ : calcd for  $C_6H_{12}N_6^+$ : 168.1118  $[M]^+$ ; found: 168.1071.

**2,5-Dibromopyrazine (18)**: Prepared according to a literature procedure.<sup>[10]</sup>  $^1H$  NMR (400 MHz,  $CDCl_3$ ):  $\delta = 8.47$  ppm (s, 2H);  $^{13}C$  NMR (100 MHz,  $CDCl_3$ ):  $\delta = 147.45, 139.24$  ppm.

**2-Amino-5-bromopyrazine (19)**: Prepared according to a literature procedure.<sup>[9]</sup>  $^1H$  NMR (400 MHz,  $CDCl_3$ ):  $\delta = 8.06$  (s, 1H), 7.75 (s, 1H), 4.76 ppm (s, br, 1H);  $^{13}C$  NMR (100 MHz,  $CDCl_3$ ):  $\delta = 153.46, 144.12, 131.73, 126.94$  ppm.

**Crystallographic data for 1**: formula  $[Ru(C_{12}H_{12}N_4)(C_{15}H_{11}N_3)]_2[PF_6]_2$ ;  $C_{27}H_{23}N_7RuF_{12}P_2$ ;  $M_r = 6.53$ ; crystal system: monoclinic; space group:  $Cc$  (No. 9),  $a = 12.721(12)$ ,  $b = 12.329(12)$ ,  $c = 20.29(2)$  Å;  $\alpha = 90$ ,  $\beta = 101.0(2)$ ,  $\gamma = 90^\circ$ ;  $V = 3124(6)$  Å<sup>3</sup>;  $Z = 4$ ;  $\rho_{calcd} = 1.779$  g cm<sup>-3</sup>;  $\mu(MoK\alpha) = 0.709$  mm<sup>-1</sup>;  $F(000) = 1664$ ; crystal size  $0.04 \times 0.05 \times 0.06$  mm; temperature 173 K;  $MoK\alpha$  radiation  $\lambda = 0.71073$  Å;  $2.3 \leq \theta \leq 41.0^\circ$ ; dataset:  $-19 \leq h \leq 19$ ;  $-19 \leq k \leq 19$ ;  $-30 \leq l \leq 31$ ; total unique data,  $R(int) = 22766, 12252, 0.069$ ; observed data  $[I > 2.0\sigma(I)]$ : 9238;  $N_{ref} = 12252$ ,  $N_{par} = 431$ ;  $R = 0.0858$ ,  $wR2 = 0.2333$ ,  $S = 1.09$ ; flack  $x = 0.02(5)$ ; minimum and maximum residual density:  $-2.35, 1.65$  e Å<sup>-3</sup>.

**Crystallographic data of 2**: formula  $[Ru_2(C_{18}H_{18}N_8)(C_{15}H_{11}N_3)_2] \cdot [PF_6]_4 \cdot 4 CH_3CN$ ;  $C_{56}H_{52}F_{24}N_{18}P_4Ru_2$ ; formula weight: 1759.18; crystal system: monoclinic; space group:  $C2/c$  (No. 15),  $a = 18.3090(4)$ ,  $b = 25.9760(6)$ ,  $c = 16.7000(4)$  Å;  $\alpha = 90$ ,  $\beta = 122.0311(13)$ ,  $\gamma = 90^\circ$ ;  $V = 6733.3(3)$  Å<sup>3</sup>;  $Z = 4$ ;  $\rho_{calcd} = 1.735$  g cm<sup>-3</sup>;  $\mu(MoK\alpha) = 0.664$  mm<sup>-1</sup>;  $F(000) = 3512$ ; crystal size  $0.08 \times 0.10 \times 0.12$  mm; temperature 173 K;  $MoK\alpha$  radiation  $\lambda = 0.71073$  Å;  $2.6 \leq \theta \leq 30.0^\circ$ ; dataset:  $-25 \leq h \leq 25$ ;  $-36 \leq k \leq 33$ ;  $-23 \leq l \leq 23$ ; total unique data,  $R(int) = 17098, 9781, 0.045$ ; observed data  $[I > 2.0\sigma(I)]$ : 7156;  $N_{ref} = 9781$ ,  $N_{par} = 470$ ;  $R = 0.0531$ ,  $wR2 = 0.1472$ ,  $S = 1.02$ ; minimum and maximum residual density:  $-0.78, 0.97$  e Å<sup>-3</sup>.

CCDC-710685 (**1**) and CCDC-710684 (**2**) contain the supplementary crystallographic data for this paper. These data can be obtained free of charge from The Cambridge Crystallographic Data Centre via [www.ccdc.cam.ac.uk/data\\_request/cif](http://www.ccdc.cam.ac.uk/data_request/cif).

## Acknowledgements

We acknowledge André de Cian and Nathalie Kyritsakas for recording the data and solving the structure of complex **2**. We acknowledge the European Synchrotron Radiation Facility for provision of synchrotron radiation facilities and we thank Dr. Gavin Vaughan for recording the data of complex **1** (ESRF experiment CH-2474, beamline ID11). We wish also to thank Lionel Allouche for DOSY NMR, Patrick Wehrung, Dr. Raymonde Baltenweck-Guyot, and Romain Carrière for mass spectrometry analyses, Dr. Juan Ramirez for helpful discussions, Prof. Frédérique Loiseau for preliminary redox experiments, and Prof. Alberto Juris for assistance in performing near-infrared luminescence experiments.

- [1] a) J.-M. Lehn, *Supramolecular Chemistry—Concepts and Perspectives*, VCH, Weinheim, **1995**; b) M. Ruben, J. Rojo, F. J. Romero-Salguero, L. H. Uppadine, J.-M. Lehn, *Angew. Chem.* **2004**, *116*, 3728; *Angew. Chem. Int. Ed.* **2004**, *43*, 3644, and references therein.
- [2] a) A.-M. Stadler, F. Puntoriero, S. Campagna, N. Kyritsakas, R. Welter, J.-M. Lehn, *Chem. Eur. J.* **2005**, *11*, 3997; b) F. Loiseau, F. Nastasi, A.-M. Stadler, S. Campagna, J.-M. Lehn, *Angew. Chem.* **2007**, *119*, 6256; *Angew. Chem. Int. Ed.* **2007**, *46*, 6144.
- [3] a) G. S. Hanan, C. R. Arana, J.-M. Lehn, D. Fenske, *Angew. Chem.* **1995**, *107*, 1191; *Angew. Chem. Int. Ed.* **1995**, *34*, 1122; b) G. S. Hanan, C. R. Arana, J.-M. Lehn, G. Baum, D. Fenske, *Chem. Eur. J.* **1996**, *2*, 1292; c) B. Hasenknopf, J. Hall, J.-M. Lehn, V. Balzani, A. Credi, S. Campagna, *New J. Chem.* **1996**, *20*, 725; d) P. Ceroni, A. Credi, V. Balzani, S. Campagna, G. S. Hanan, C. R. Arana, J.-M. Lehn, *Eur. J. Inorg. Chem.* **1999**, 1409; e) D. Brown, S. Muranjan, Y. Jang, R. Thummel, *Org. Lett.* **2002**, *4*, 1253; f) D. Brown, R. Zong, R. P. Thummel, *Eur. J. Inorg. Chem.* **2004**, 3269; g) For related  $Ru^{II}$  complexes used for water oxidation, see: R. Zong, R. P. Thummel, *J. Am. Chem. Soc.* **2005**, *127*, 12802.
- [4] M. M. Castano-Briones, A. P. Bassett, L. L. Meason, P. R. Ashton, Z. Pikramenou, *Chem. Commun.* **2004**, 2832.
- [5] a) M. Schmittel, V. Kalsani, J. W. Bats, *Inorg. Chem.* **2005**, *44*, 4115; b) V. Kalsani, H. Bodenstedt, D. Fenske, M. Schmittel, *Eur. J. Inorg. Chem.* **2005**, 1841; c) M. Schmittel, V. Kalsani, R. S. K. Kishore, H. Cölfen, J. W. Bats, *J. Am. Chem. Soc.* **2005**, *127*, 11544; d) J. Ramirez, A.-M. Stadler, G. Rogez, M. Drillon, J.-M. Lehn, *Inorg. Chem.* **2009**, *48*, 2456.

- [6] J.-L. Schmitt, A.-M. Stadler, N. Kyritsakas, J.-M. Lehn, *Helv. Chim. Acta* **2003**, *86*, 1598.
- [7] A.-M. Stadler, N. Kyritsakas, R. Graff, J.-M. Lehn, *Chem. Eur. J.* **2006**, *12*, 4503.
- [8] M. A. Baldo, G. Chessa, G. Marangoni, B. Pitteri, *Synthesis* **1987**, 720.
- [9] D. A. De Bie, A. Ostrowica, G. Geurtsen, H. C. Van Der Plas, *Tetrahedron* **1988**, *44*, 2977.
- [10] R. C. Ellingson, R. L. Henry, *J. Am. Chem. Soc.* **1949**, *71*, 2798.
- [11] M. Hasegawa, Y. Asusuki, F. Susuki, H. Nakanishi, *J. Polym. Sci. Part A-1* **1969**, *7*, 743–752.
- [12] a) R. H. Wiley, US Patent 4260757, **1981**; b) R. H. Wiley, *J. Macromol. Sci. Part A* **1987**, *24*, 1183.
- [13] See, for example: a) C. S. Poss, S. L. Schreiber, *Acc. Chem. Res.* **1994**, *27*, 9; b) S. R. Magnuson, *Tetrahedron* **1995**, *51*, 2167.
- [14] K. M. Gardinier, R. G. Khoury, J.-M. Lehn, *Chem. Eur. J.* **2000**, *6*, 4124.
- [15] B. P. Sullivan, J. M. Calvert, T. J. Meyer, *Inorg. Chem.* **1980**, *19*, 1404.
- [16] a) T. J. Cho, C. N. Moorefield, S.-H. Hwang, P. Wang, L. A. Godínez, E. Bustos, G. R. Newkome, *Eur. J. Org. Chem.* **2006**, 4193; b) L. Al-louche, A. Marquis, J.-M. Lehn, *Chem. Eur. J.* **2006**, *12*, 7520.
- [17] F. Puntoriero, S. Campagna, A.-M. Stadler, J.-M. Lehn, *Coord. Chem. Rev.* **2008**, *252*, 2480.
- [18] a) A. Juris, V. Balzani, F. Barigelletti, S. Campagna, P. Belser, A. von Zelewsky, *Coord. Chem. Rev.* **1988**, *84*, 85; b) J.-P. Sauvage, J. P. Collin, J. C. Chambron, S. Guillerez, C. Coudret, V. Balzani, F. Barigelletti, L. De Cola, L. Flamigni, *Chem. Rev.* **1994**, *94*, 993; c) V. Balzani, A. Juris, M. Venturi, S. Campagna, S. Serroni, *Chem. Rev.* **1996**, *96*, 759.
- [19] Redox splitting can be related to intercomponent electronic coupling only for weakly coupled systems, that is when valence is vibrationally trapped (Classes I and II of the Robin–Day mixed-valence systems).<sup>[20]</sup> For strongly interacting species (Class III), valence delocalization occurs and the potential separation between first and second oxidation processes assumes different meanings. To discriminate between weakly and strongly coupled systems, intervalence transfer bands of mono-oxidized species, investigated by spectroelectrochemistry, are quite useful. We performed spectroelectrochemistry experiments for **2**, and found (see the Supporting Information to reference [2b]) that this species exhibits behavior belonging to the transition regime between Class II and Class III, a borderline regime defined quite recently.<sup>[21,22]</sup> In other words, in **2**, valence delocalization could occur to some extent, but referring to metal–metal interaction as the origin of oxidation splitting is still valid.
- [20] a) M. B. Robin, P. Day, *Adv. Inorg. Chem. Radiochem.* **1968**, *10*, 247; b) D. E. Richardson, H. Taube, *J. Am. Chem. Soc.* **1983**, *105*, 40; c) C. Creutz, *Prog. Inorg. Chem.* **1983**, *30*, 1.
- [21] a) C. Lambert, G. Nöll, *J. Am. Chem. Soc.* **1999**, *121*, 8434; b) S. F. Nelsen, *Chem. Eur. J.* **2000**, *6*, 581; c) K. D. Demadis, C. M. Harts-horn, T. J. Meyer, *Chem. Rev.* **2001**, *101*, 2655.
- [22] a) B. S. Brunschwig, C. Creutz, N. Sutin, *Chem. Soc. Rev.* **2002**, *31*, 168; b) D. M. D'Alessandro, F. R. Keene, *Chem. Soc. Rev.* **2006**, *35*, 424.
- [23] If this was the case, the first reduction potential of **3a**, containing the pyrazine-based unit, should be less negative than that of **3b**, containing the pyrimidine-based unit: the reverse was found experimentally.
- [24] S. Campagna, F. Puntoriero, F. Nastasi, G. Bergamini, V. Balzani, *Top. Curr. Chem.* **2007**, *280*, 117.
- [25] T. J. Meyer, *Pure Appl. Chem.* **1986**, *58*, 1193, and references therein.
- [26] Y. Chen, T. J. Meyer, *Chem. Rev.* **1998**, *98*, 1439.
- [27] See, for example: a) A. Mamo, I. Stefio, A. Poggi, C. Tringali, C. Di Pietro, S. Campagna, *New J. Chem.* **1997**, *21*, 1173; b) J. A. Tread-way, G. F. Strouse, R. R. Ruminski, T. J. Meyer, *Inorg. Chem.* **2001**, *40*, 4508; c) S. M. Draper, D. J. Gregg, E. R. Schofield, W. R. Browne, M. Duati, J. G. Vos, P. Passaniti, *J. Am. Chem. Soc.* **2004**, *126*, 8694; d) S. D. Bergman, D. Gut, M. Kol, C. Sabatini, A. Barbieri, F. Barigelletti, *Inorg. Chem.* **2005**, *44*, 7943; e) M. I. J. Polson, F. Loiseau, S. Campagna, G. S. Hanan, *Chem. Commun.* **2006**, 1301.
- [28] Near-infrared emission has been reported for species containing Ru<sup>II</sup> subunits connected to Os<sup>[29a]</sup> or Nd units,<sup>[29b]</sup> but in those cases the emission was Os-based or Nd-based and the Ru units played the role of energy-transfer donors.
- [29] a) A. Juris, V. Balzani, S. Campagna, G. Denti, S. Serroni, G. Frei, H. U. Güdel, *Inorg. Chem.* **1994**, *33*, 1491; b) C. Giansante, P. Ceroni, V. Balzani, F. Vögtle, *Angew. Chem.* **2008**, *120*, 5502; *Angew. Chem. Int. Ed.* **2008**, *47*, 5422.
- [30] The structure of an emission spectrum is the result of the Franck–Condon factors for radiative transition decay, which are connected to the geometrical distortion ( $\Delta Q$ ) between the ground and excited states.<sup>[31,32]</sup> A single-mode Franck–Condon analysis of the emission spectra,<sup>[32]</sup> using Equation (1), allows parameters  $E_0$ ,  $\hbar\omega$ ,  $S_M$ , and  $\Delta\nu_{1/2}$  to be obtained.
- $$I(\tilde{\nu}) = \sum_{x=0}^5 \left[ \left( \frac{E_0 - x\hbar\omega}{E_0} \right)^3 \left( \frac{S^x}{x!} \right) \left( \exp \left[ -4 \ln 2 \left( \frac{\tilde{\nu} - E_0 + x\hbar\omega}{\Delta\nu_{1/2}} \right)^2 \right] \right) \right] \quad (1)$$
- In Equation (1),  $\tilde{\nu}$  is the relative emission intensity at energy  $\tilde{\nu}$  (in  $\text{cm}^{-1}$ ),  $E_0$  is the energy of the zero–zero transition (i.e., the energy of the emitting <sup>3</sup>MLCT state),  $\hbar\omega$  is the average of the medium frequency acceptor modes coupled to the radiative transition,  $x$  is the quantum number of such an averaged medium frequency mode that serves as the final vibronic states ( $x$  is usually limited to 5),  $\Delta\nu_{1/2}$  is the half-width of the individual vibronic bands, and  $S$  is the electron–vibrational coupling constant (Huang–Rhys factor).<sup>[32]</sup> The  $S$  parameter is linked to  $\Delta Q$  by Equation (2).
- $$S = \frac{1}{2} \frac{M\omega}{\hbar} (\Delta Q)^2 \quad (2)$$
- In Equation (2),  $M$  is the reduced mass of the oscillator, and  $\omega$  is the frequency of the dominant vibrational mode. In general, a highly structured emission spectrum indicates a low value of  $S$ , and therefore of  $\Delta Q$ . For transition-metal complexes, only ligand-centered (LC) or metal-to-ligand charge-transfer (MLCT) emissions normally exhibit small values of  $\Delta Q$  and can therefore show structured emission spectra.<sup>[19,24,33]</sup>
- [31] M. Klessinger, J. Michl, *Excited States and Photochemistry of Organic Molecules*, Wiley-VCH, Weinheim, **1995**.
- [32] a) R. Englman, J. Jortner, *J. Mol. Phys.* **1970**, *18*, 145; b) B. R. Henry, W. Siebrand in *Organic Molecular Photophysics, Vol. 1* (Ed.: J. B. Birks), Wiley, New York, **1973**; c) J. V. Caspar, E. M. Kober, B. P. Sullivan, T. J. Meyer, *J. Am. Chem. Soc.* **1982**, *104*, 630; d) J. V. Caspar, T. J. Meyer, *J. Am. Chem. Soc.* **1983**, *105*, 5583; e) J. P. Claude, T. J. Meyer, *J. Phys. Chem.* **1995**, *99*, 51; f) N. H. Damrauer, T. R. Boussie, M. Devenney, J. K. McCusker, *J. Am. Chem. Soc.* **1997**, *119*, 8253; g) J. A. Treadway, G. F. Strouse, R. R. Ruminski, T. J. Meyer, *Inorg. Chem.* **2001**, *40*, 4508; h) Y.-Q. Fang, N. J. Taylor, F. Laverdière, G. S. Hanan, F. Loiseau, F. Nastasi, S. Campagna, H. Nierengarten, E. Leize-Wagner, A. Van Dorselaer, *Inorg. Chem.* **2007**, *46*, 2854.
- [33] G. A. Crosby, *Acc. Chem. Res.* **1975**, *8*, 231.
- [34] a) *Rare-Earth Doped Fiber Lasers and Amplifiers* (Ed.: M. J. F. Digonnet), Marcel Dekker, New York, **1993**; b) J. Nilsson, W. A. Clarkson, R. Selvas, J. K. Sahu, P. W. Turner, S.-U. Alam, A. B. Grudin, *Opt. Fiber Technol.* **2004**, *10*, 5.

Received: March 10, 2009

Revised: January 7, 2010

Published online: April 8, 2010